Modelling last glacial cycle ice dynamics in the Alps

Julien Seguinot[1], Guillaume Jouvet[1], Matthias Huss[1], Martin Funk[1], Susan Ivy-Ochs[2], and
Frank Preusser[3]

[1]Laboratory of Hydraulics, Hydrology and Glaciology, ETH Zürich, Switzerland
[2]Laboratory of Ion Beam Physics, ETH Zürich, Switzerland
[3]Institute of Earth and Environmental Sciences, University of Freiburg, Germany

Correspondence to: J. Seguinot (seguinot@vaw.baug.ethz.ch)

Abstract.

The European Alps, cradle of pioneer glacial studies, are one of the regions where geological markers of past glaciations are most abundant and well-studied. Such conditions make the region ideal for testing numerical glacier models based on simplified ice flow physics against field-based reconstructions, and vice-versa.

Here, we use the Parallel Ice Sheet Model (PISM) to model the entire last glacial cycle (120–0 ka) in the Alps, using horizontal resolutions of 2 and 1 km and up to 576 processors. Climate forcing is derived using present-day climate data from WorldClim and the ERA-Interim reanalysis, and time-dependent temperature offsets from multiple palaeo-climate proxies, among which only the EPICA ice core record yields glaciation during marine oxygen isotope stages 4 (69–62 ka) and 2 (34–18 ka) spatially and temporally consistent with the geological reconstructions, while the other records used result in excessive early glacial cycle ice cover and a late Last Glacial Maximum. Despite the low variability of this Antarctic-based climate forcing, our simulation depicts a highly dynamic ice sheet, showing that Alpine glaciers may have advanced many times over the foreland during the last glacial cycle. Ice flow patterns during peak glaciation are largely governed by subglacial topography but include occasional transfluences and self-sustained ice domes. Modelled maximum ice surface is 861 m higher than observed trimline elevations in the upper Rhone Valley, yet our simulation predicts little erosion at high elevation due to cold-based ice. Finally, the Last Glacial Maximum advance, often considered synchronous, is here modelled as a time-transgressive event, with some glacier lobes reaching their maximum as early as 27 ka, and some as late as 21 ka.

1 Introduction

For nearly 300 years, montane people and early explorers of the European Alps learned to read the geomorphological imprint left by glaciers in the landscape, and to understand that glaciers had once been more extensive than today (e.g., Windham and Martel, 1744, p. 21). Contemporaneously, it was also observed in the Alps that glaciers move by a combination of meltwater-induced *sliding* at the base (de Saussure, 1779, §532), and viscous *deformation* within the ice body (Forbes, 1846). As glaciers flow and slide across their bed, they transport rock debris and erode the landscape, thereby leaving geomorphological traces of their former presence. In the mid-nineteenth century, more systematic studies of glacial features showed that Alpine glaciers extended well below their current margins (Venetz, 1821) and even onto the Alpine foreland (Charpentier, 1841), yielding the

idea that, under colder temperatures, expansive *ice sheets* had once covered much of Europe and North America (Agassiz, 1840).

However, this glacial theory did not gain general acceptance until the discovery and exploration of the two present-day ice sheets on Earth, the Greenland and Antarctic ice sheets, provided a modern analogue for the proposed European and North

5　American ice sheets. Although it was long unclear whether there had been a single or multiple glaciations, this controversy ended with the large-scale mapping of two distinct moraine systems in North America (Chamberlin, 1894). In the European Alps, the systematic classification of the glaciofluvial terraces on the northern foreland later indicated that there had been at least four major glaciations in the Alps (Penck and Brückner, 1909). More recent studies of glaciofluvial stratigraphy in the foreland indicate at least 15 glaciations (Schlüchter, 1988; Ivy-Ochs et al., 2008; Preusser et al., 2011).

10　From the mid-twentieth century, palaeo-climate records extracted from deep sea sediments and ice cores have provided a much more detailed picture of the Earth's environmental history (e.g., Emiliani, 1955; Shackleton and Opdyke, 1973; Dansgaard et al., 1993; Augustin et al., 2004), indicating several tens of glacial and interglacial periods. During the last 800 ka before present, these *glacial cycles* have succeeded each other with a periodicity about 100 ka (Hays et al., 1976; Augustin et al., 2004). Nevertheless, this global signal is largely governed by the North American and Eurasian ice sheet complexes. It

15　is thus unclear whether glacier advances and retreats in the Alps were in pace with global sea-level fluctuations. Besides, the landform record is typically sparse in time and, most often, spatially incomplete. Palaeo-ice sheets did not leave a continuous imprint on the landscape, and much of this evidence has been overprinted by subsequent glacier re-advances and other geomorphological processes (e.g., Kleman, 1994; Kleman et al., 2006, 2010). Dating uncertainties typically increase with age, such that dated reconstructions are strongly biased towards later glaciations (Heyman et al., 2011). In the European Alps, although

20　sparse geological traces indicate that the last glacial cycle may have comprised two or three cycles of glacier growth and decay (Preusser, 2004; Ivy-Ochs et al., 2008), most glacial features currently left on the foreland present a record of the last major glaciation of the Alps, dating from the *Last Glacial Maximum* (LGM).

The spatial extent and thickness of Alpine glaciers during the LGM, an integrated footprint of thousands of years of climate history and glacier dynamics, have been reconstructed from moraines and trimlines across the mountain range (e.g., Penck and

25　Brückner, 1909; Castiglioni, 1940; van Husen, 1987; Bini et al., 2009; Coutterand, 2010). The assumption that trimlines, the upper limit of glacial erosion, represent the maximum ice surface elevation, has been repeatedly invalidated in other glaciated regions of the globe (e.g., Kleman, 1994; Kleman et al., 2010; Fabel et al., 2012). Although no evidence for cold-based glaciation has been reported in the Alps to date, it is supported by numerical modelling (Haeberli and Schlüchter, 1987, Fig. 3). Alpine ice flow patterns were primarily controlled by subglacial topography, but there is evidence for flow accross

30　major mountain passes (e.g., Coutterand, 2010; Kelly et al., 2004; van Husen, 2011), and self-sustained ice domes (Bini et al., 2009). Finally, the timing of the LGM in the Alps (Ivy-Ochs et al., 2008; Monegato et al., 2017) is in good agreement with the maximum expansion of continental ice sheets recorded by the Marine Oxygen Isotope Stage (MIS) 2 (29–14 ka; Lisiecki and Raymo, 2005). Regional variation between different piedmont lobes exists (Wirsig et al., 2016, Fig. 5), but it is unclear whether this relates to climate or glacier dynamics (Monegato et al., 2017) or uncertainties in the dating methods.

Although the glacial history of the European Alps has been studied for nearly three hundred years, it thus remains incompletely known (1) what climate evolution lead to the known maximum ice limits, (2) to which extent ice flow was controlled by subglacial topography, (3) what drove the different response of the individual lobes, (4) how far above the trimline was the ice surface located, and (5) how many advances occurred during the last glacial cycle.

5 Here, we use the Parallel Ice Sheet Model (PISM, the PISM authors, 2017), a numerical ice sheet model that approximates glacier sliding and deformation (Sect. 2), to model Alpine glacier dynamics through the last glacial cycle (120–0 ka), a period for which palaeo-temperature proxies are available, albeit non regional. In an attempt to analyse the longstanding questions outlined above, we test the model sensitivity to multiple palaeo-climate forcing (Sect. 3), and then explore the modelled glacier dynamics at high resolution for the optimal forcing (Sect. 4).

10 2 Ice sheet model set-up

2.1 Overview

We use the Parallel Ice Sheet Model (PISM, development version e9d2d1f), an open source, finite difference, shallow ice sheet model (the PISM authors, 2017). The model requires input on initial bedrock and glacier topographies, geothermal heat flux and climate forcing. It computes the evolution of ice extent and thickness over time, the thermal and dynamic states of the ice

15 sheet, and the associated lithospheric response. The model set-up used here was previously developed and tested on the former Cordilleran ice sheet (Seguinot, 2014; Seguinot et al., 2014, 2016) and subsequently adapted for steady climate (Becker et al., 2016) and regional (Jouvet et al., 2017) applications to the European Alps.

Ice deformation follows temperature and water-content dependent creep (Sect. 2.2). Basal sliding follows a pseudo-plastic law where the yield stress accounts for till dilatation under high water pressure (Sect. 2.3). Bedrock topography is deflected

20 under the ice load (Sect. 2.4). Surface mass balance is computed using a positive degree-day (PDD) model (Sect. 2.5). Climate forcing is provided by a monthly climatology from interpolated observational data (WorldClim; Hijmans et al., 2005) and the European Centre for Medium-Range Weather Forecasts Reanalysis Interim (ERA-Interim; Dee et al., 2011), amended with temperature lapse-rate corrections (Sect. 2.6), time-dependent temperature offsets, and in some cases, time-dependent palaeo-precipitation reductions (Sect. 3).

25 Each simulation starts from assumed present-day ice thickness and equilibrium ice and bedrock temperature at 120 ka, and runs to the present. Our modelling domain of 900 by 600 km encompasses the entire Alpine range (Fig. 1). The simulations were run on two distinct grids, using horizontal resolutions of 2 and 1 km, respectively. All parameter values are summarized in Table 1.

2.2 Ice rheology

30 Ice sheet dynamics are typically modelled using a combination of internal deformation and basal sliding. PISM is a shallow ice sheet model, which implies that the balance of stresses is approximated based on their predominant components. The Shallow

Shelf Approximation (SSA) is combined with the Shallow Ice Approximation (SIA) by adding velocity solutions of the two approximations (Winkelmann et al., 2011, Eqs. 7–9 and 15). Although this heuristic approach is inaccurate in the transition zone where both vertical shear and longitudinal stretch are significant, it was shown to effectively approximate complex ice field flow dynamics over mountainous topographies similar to that of the European Alps (Golledge et al., 2012; Ziemen et al.,

5   2016). This hybrid scheme is computationally much more efficient than a fully three-dimensional model (e.g., Cohen et al., 2017) with which simulations of the scale presented here would not be feasible.

Ice deformation is governed by the constitutive law for ice (Glen, 1952; Nye, 1953). Ice softness depends on ice temperature, pressure, and water content, through an enthalpy scheme (Table 1; Aschwanden et al., 2012) and a piece-wise Arrhenius-type rheology representative of Holocene polar ice (Table 1; Cuffey and Paterson, 2010, p. 77). The englacial water fraction is

10   capped at a maximum value of 0.01, above which no measurements are available (Lliboutry and Duval, 1985; Greve, 1997, Eq. 5.7).

Surface air temperature derived from the climate forcing (Sects. 2.6, 3.1) provides the upper boundary condition to the ice enthalpy model. Temperature is computed in the ice and in the bedrock down to a depth of 3 km below the glacier base, where it is conditioned by a lower boundary geothermal heat flux estimate from multiple geothermal proxies (Goutorbe et al., 2011,

15   similarity method; Fig. 1a).

2.3   Basal sliding

A pseudo-plastic sliding law relates the bed-parallel shear stresses to the sliding velocity. The yield stress is modelled using the Mohr–Coulomb criterion using a constant basal friction angle (Table 1). Effective pressure is related to the ice overburden stress and the modelled amount of subglacial water, using a formula derived from laboratory experiments with till extracted

20   from the base of Ice Stream B in West Antarctica (Table 1; Tulaczyk et al., 2000; Bueler and van Pelt, 2015). When the till becomes saturated, additional melt water is assumed to drain off instantaneously.

2.4   Basal topography

The initial basal topography is bilinearly interpolated from the hole-filled, Shuttle Radar Topography Mission (SRTM) data with a resolution of 30 arc-sec (Fig. 1b; Jarvis et al., 2008). These data include post-glacial sediment fills and lakes surface

25   topography. However, they were corrected for an estimation of present-day ice thickness based on modern glacier outlines, surface topography and simplified ice physics (Fig. 1c; Huss and Farinotti, 2012).

Basal topography responds to ice load following a bedrock deformation model that includes local isostasy, elastic lithosphere flexure and viscous asthenosphere deformation in an infinite half-space (Lingle and Clark, 1985; Bueler et al., 2007). Model
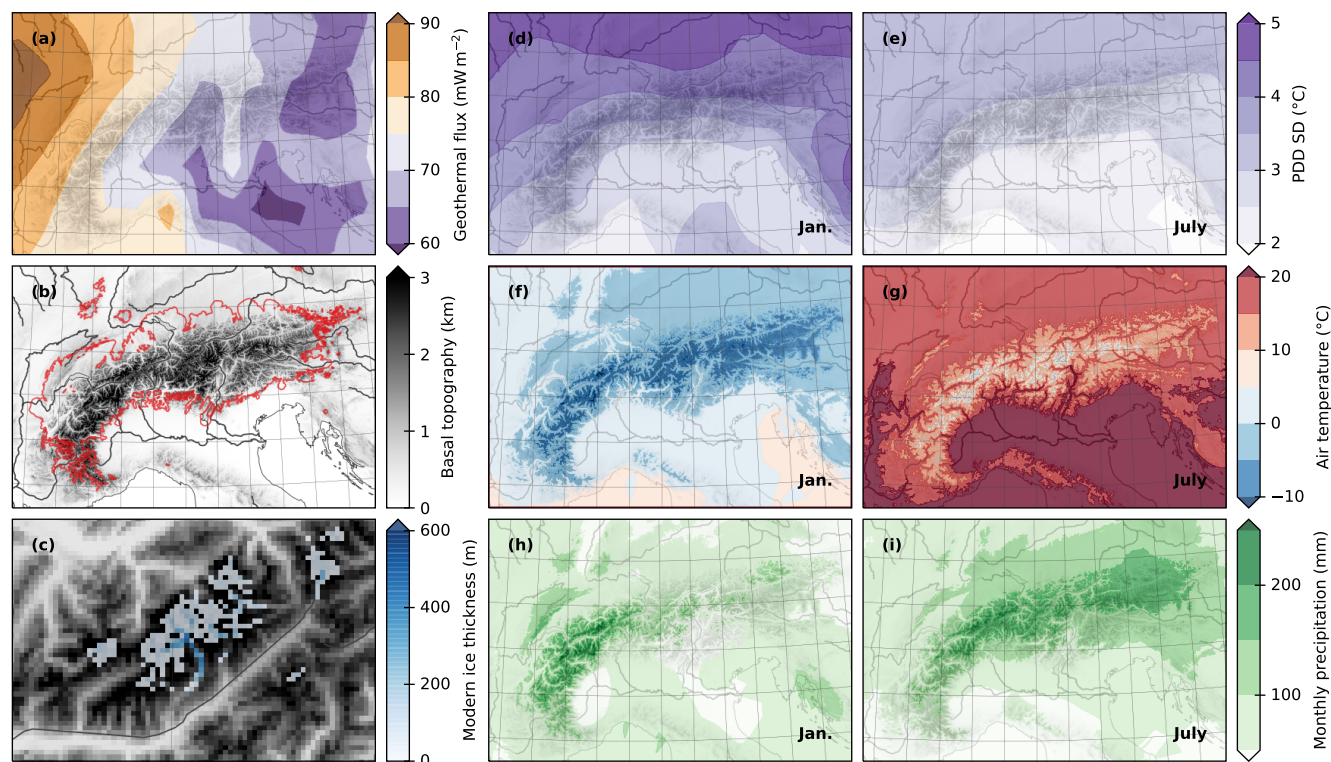
The Cryosphere
Discussions

Open Access

EGU

Figure 1. (a) Geothermal heat flow from applying the similarity method to multiple geophysical proxies (Goutorbe et al., 2011) used as a boundary condition to the bedrock thermal model 3 km below the ice-bedrock interface. **(b)** Initial basal topography from SRTM (Jarvis et al., 2008) and geomorphological reconstruction of Last Glacial Maximum Alpine glacier extent (solid red line, Ehlers et al., 2011). **(c)** Extract from the estimated of present-day ice thickness (Huss and Farinotti, 2012) substracted from the SRTM topography and aggregated to a 1 km horizontal resolution. **(d)** Modern January and **(e)** July standard deviation (Seguinot, 2013) of daily mean temperature from the ERA-Interim (1979–2012; Dee et al., 2011) from the reference monthly climatology used to force the surface mass balance (PDD) component of the ice sheet model. **(f)** Modern January and **(g)** July mean near-surface air temperature, and **(h, i)** precipitation from WorldClim (1960–1990; Hijmans et al., 2005).

parameters were set according to results from glacial isostatic adjustment modelling of deglacial rebound in the Alps most closely reproducing observed modern uplift rates (Mey et al., 2016, Supplementary Fig. 7).[1]

2.5 Surface mass balance

Ice surface accumulation and ablation are computed from monthly mean near-surface air temperature, T_m, monthly standard deviation of near-surface air temperature, σ, and monthly precipitation, P_m, using a temperature-index model (e.g., Hock, 2003). Accumulation is equal to precipitation when air temperatures are below $0\,°\mathrm{C}$, and decreases to zero linearly with

5   temperatures between 0 and $2\,°\mathrm{C}$. Ablation is computed from PDD, the integral of temperatures above $0\,°\mathrm{C}$.

The PDD computation accounts for stochastic temperature variations by assuming a normal temperature distribution of standard deviation, σ, around the expected value, T_m. It is expressed by an error-function formulation (Calov and Greve, 2005) which is numerically approximated using week-long sub-intervals. In order to account for the effects of spatial and seasonal variations of temperature variability (Seguinot, 2013), σ is computed from ERA-Interim daily temperature values

10   from 1979 to 2012 (Mesinger et al., 2006), including variability associated with the seasonal cycle (Seguinot, 2013), and bilinearly interpolated to the model grids (Fig. 1d and e). Degree-day factors for snow and ice melt are set to values used in the European Ice Sheet Modelling INiTiative (Table 1; EISMINT, Huybrechts, 1998).

2.6 Reference climate forcing

Climate forcing driving ice sheet simulations consists of a present-day monthly climatology, $\{T_\mathrm{m0}, P_\mathrm{m0}\}$, modified by temper-

15   ature lapse-rate corrections, ΔT_LR, temperature offset time series, ΔT_TS, and time-dependent palaeo-precipitation corrections, Ψ_PP:

$$T_\mathrm{m}(t,x,y) = T_\mathrm{m0}(x,y) + \Delta T_\mathrm{LR}(t,x,y) + \Delta T_\mathrm{TS}(t), \tag{1}$$

$$P_\mathrm{m}(t,x,y) = P_\mathrm{m0}(x,y) \cdot \Psi_\mathrm{PP}(t), \tag{2}$$

The present-day monthly climatology was bilinearly interpolated from near-surface air temperature and precipitation rate fields

20   from WorldClim (Hijmans et al., 2005), representative of the period 1960 to 1990. Modern climate of the European Alps is characterised by a north-south gradient in winter and summer air temperatures (Fig. 1f and g), and an east-west gradient in winter precipitation (Fig. 1h) which is reversed in summer (Fig. 1h). WorldClim data were selected as an input to the ice sheet model because they incorporate observations from the dense weather station network of central Europe (Hijmans et al., 2005, Fig. 1). Besides, WorldClim data were previously used as climate forcing for PISM to model the LGM extent of the former

25   Cordilleran ice sheet in good agreement with geological evidence along the southern margin (Seguinot et al., 2014) where weather station density is lower than in the Alps. Finally, the last glacial cycle Alpine glaciers did not extend over marine areas where WorldClim data is missing.

---

[1]Lithosphere rigidity was computed using the erroneous formula, $D = YE^3/12(1-\nu)$, in Mey et al. (2016). The correct formula is $D = YE^3/12(1-\nu^2)$. Using the Young's modulus, $Y = 100\,\mathrm{GPa}$, and the Poisson ratio, $\nu = 0.25$ (Mey et al., 2016), our simulations effectively use an elastic thickness of the lithosphere of $E = 52.4\,\mathrm{km}$, instead of the $50\,\mathrm{km}$ value used by Mey et al. (2016), introducing in a small change in the lenght scale of bedrock deformation well within uncertainties (Mey et al., 2016).

The temperature lapse-rate corrections, ΔT_{LR}, are computed as a function of ice surface elevation, s, using the SRTM topography shipped with WorldClim as a reference, b_{ref}:

$$\Delta T_{\mathrm{LR}}(t,x,y) = -\gamma[s(t,x,y) - b_{\mathrm{ref}}] \tag{3}$$

$$= -\gamma[h(t,x,y) + b(t,x,y) - b_{\mathrm{ref}}], \tag{4}$$

thus accounting for the evolution of ice thickness, $h = s - b$, on the one hand, and for differences between the basal topography of the ice flow model, b, and the WorldClim reference topography, b_{ref}, on the other hand. All simulations use an annual temperature lapse rate of $\gamma = 6\,\mathrm{K\,km^{-1}}$.

3 Palaeo-climate forcing

In this section, we analyze the model sensitivity to palaeo-climate forcing through the last glacial cycle, using three palaeo-temperature records (Sect. 3.1) and two parametrizations of palaeo-precipitation (Sect. 3.2), in terms of modelled evolution of total ice volume (Sect. 3.3) and glaciated area during MIS 2 and 4 (Sect. 3.4).

These simulations use a horizontal resolution of 2 km. The vertical grid consists of 31 temperature layers in the bedrock and up to 126 enthalpy layers in the ice, corresponding to vertical resolutions of 100 and 40 m, respectively. Simulations ran for two to four days using 144 processors.

3.1 Palaeo-temperature forcing

Temperature offset time-series, ΔT_{TS}, are derived from palaeo-temperature proxy records from the Greenland Ice Core Project (GRIP; Dansgaard et al., 1993), the European Project for Ice Coring in Antarctica (EPICA; Jouzel et al., 2007), and an oceanic sediment core from the Iberian margin (MD01-2444; Martrat et al., 2007). Palaeo-temperature anomalies from the GRIP record are calculated from oxygen isotope ($\delta^{18}\mathrm{O}$) measurements using a quadratic equation (Johnsen et al., 1995),

$$\Delta T_{\mathrm{TS}}(t) = -11.88[\delta^{18}\mathrm{O}(t) - \delta^{18}\mathrm{O}(0)]$$
$$-0.1925[\delta^{18}\mathrm{O}(t)^2 - \delta^{18}\mathrm{O}(0)^2], \tag{5}$$

while temperature reconstructions from the EPICA and MD01-2444 records are provided as such. For each proxy record used and each of the parameter set-ups used in the sensitivity tests, palaeo-temperature anomalies are scaled linearly (Table 2, Fig. 2a) so that the modelled cumulative glaciated area during MIS 2 (29–14 ka) and within a rectangular region covering the Rhine glacier piedmont lobe (Fig. 3a, black rectangle) is consistent with the glaciated area of the geological reconstruction (Ehlers et al., 2011).

3.2 Palaeo-precipitation forcing

Finally, in some simulations (hereafter labelled PP), precipitation was reduced with air temperature in order to simulate the potential rarefaction of atmospheric moisture in colder climates. This was done using an empirical relationship derived from

Table 1. Parameter values used in the ice sheet model. Symbols refer to equations used by Seguinot (2014); Seguinot et al. (2016).

Not.	Name	Value	Unit	Source
Ice rheology				
ρ	Ice density	910	$\mathrm{kg\,m^{-3}}$	Aschwanden et al. (2012)
g	Standard gravity	9.81	$\mathrm{m\,s^{-2}}$	Aschwanden et al. (2012)
n	Glen exponent	3	–	Cuffey and Paterson (2010, p. 55–57)
A_c	Ice hardness coefficient cold	2.847×10^{-13}	$\mathrm{Pa^{-3}\,s^{-1}}$	Cuffey and Paterson (2010, p. 72)
A_w	Ice hardness coefficient warm	2.356×10^{-2}	$\mathrm{Pa^{-3}\,s^{-1}}$	Cuffey and Paterson (2010, p. 72)
Q_c	Flow law activation energy cold	6.0×10^4	$\mathrm{J\,mol^{-1}}$	Cuffey and Paterson (2010, p. 72)
Q_w	Flow law activation energy warm	11.5×10^4	$\mathrm{J\,mol^{-1}}$	Cuffey and Paterson (2010, p. 72)
E_SIA	SIA enhancement factor	2	–	Cuffey and Paterson (2010, p. 77)
E_SSA	SSA enhancement factor	1	–	Cuffey and Paterson (2010, p. 77)
T_c	Flow law critical temperature	263.15	K	Paterson and Budd (1982)
f	Flow law water fraction coeff.	181.25	–	Lliboutry and Duval (1985)
R	Ideal gas constant	8.31441	$\mathrm{J\,mol^{-1}\,K^{-1}}$	–
β	Clapeyron constant	7.9×10^{-8}	$\mathrm{K\,Pa^{-1}}$	Lüthi et al. (2002)
c_i	Ice specific heat capacity	2009	$\mathrm{J\,kg^{-1}\,K^{-1}}$	Aschwanden et al. (2012)
c_w	Water specific heat capacity	4170	$\mathrm{J\,kg^{-1}\,K^{-1}}$	Aschwanden et al. (2012)
k	Ice thermal conductivity	2.10	$\mathrm{J\,m^{-1}\,K^{-1}\,s^{-1}}$	Aschwanden et al. (2012)
L	Water latent heat of fusion	3.34×10^5	$\mathrm{J\,kg^{-1}\,K^{-1}}$	Aschwanden et al. (2012)
Basal sliding				
q	Pseudo-plastic sliding exponent	0.25	–	Aschwanden et al. (2013)
v_th	Pseudo-plastic threshold velocity	100	$\mathrm{m\,a^{-1}}$	Aschwanden et al. (2013)
c_0	Till cohesion	0	Pa	Tulaczyk et al. (2000)
e_0	Till reference void ratio	0.69	–	Tulaczyk et al. (2000)
C_c	Till compressibility coefficient	0.12	–	Tulaczyk et al. (2000)
δ	Minimum effective pressure ratio	0.02	–	Bueler and van Pelt (2015)
ϕ	Till friction angle	30	°	Cuffey and Paterson (2010, p. 268)
W_max	Maximum till water thickness	2	m	Bueler and van Pelt (2015)
Bedrock and lithosphere				
ρ_b	Bedrock density	3300	$\mathrm{kg\,m^{-3}}$	–
c_b	Bedrock specific heat capacity	1000	$\mathrm{J\,kg^{-1}\,K^{-1}}$	–
k_b	Bedrock thermal conductivity	3	$\mathrm{J\,m^{-1}\,K^{-1}\,s^{-1}}$	–
ν_m	Astenosphere viscosity	2.2×10^{20}	$\mathrm{Pa\,s}$	Mey et al. (2016)
ρ_m	Astenosphere density	3300	$\mathrm{kg\,m^{-3}}$	Mey et al. (2016)
D	Lithosphere flexural rigidity	1.389×10^{24}	$\mathrm{N\,m}$	Mey et al. (2016)
Surface and atmosphere				
T_s	Temperature of snow precipitation	273.15	K	–
T_r	Temperature of rain precipitation	275.15	K	–
F_s	Degree-day factor for snow	3.297×10^{-3}	$\mathrm{m\,K^{-1}\,day^{-1}}$	Huybrechts (1998)
F_i	Degree-day factor for ice	8.791×10^{-3}	$\mathrm{m\,K^{-1}\,day^{-1}}$	Huybrechts (1998)
R	Refreezing fraction	0.0	–	–
γ	Air temperature lapse rate	6×10^{-3}	$\mathrm{K\,m{-1}}$	–
ψ	Precipitation factor	0.0704	–	Huybrechts (2002)

Table 2. Palaeo-temperature proxy records and scaling factors yielding temperature offset time-series used to force the ice sheet model through the last glacial cycle (Fig. 2). f corresponds to the scaling factor adopted to yield Last Glacial Maximum ice limits in the vicinity of mapped end moraines (Fig. 3a), and $[\Delta T_{TS}]_{32}^{22}$ refers to the resulting mean temperature anomaly during the period 32 to 22 ka after scaling.

Forcing	Latitude	Longitude	Elev. (m a.s.l.)	Proxy	f	$[\Delta TS]_{32}^{22}$ (K)	Reference
GRIP					0.50	−8.2	
GRIP, PP	72°35′ N	37°38′ W	3238	$\delta^{18}O$	0.63	−10.4	Dansgaard et al. (1993)
EPICA					1.05	−9.7	
EPICA, PP	75°06′ S	123°21′ E	3233	$\delta^{18}O$	1.33	−12.2	Jouzel et al. (2007)
MD01-2444					1.84	−8.0	
MD01-2444, PP	37°34′ N	10°04′ W	−2637	$U_{37}^{K'}$	2.44	−10.6	Martrat et al. (2007)

observed accumulation rates and oxygen isotopes concentrations in the GRIP ice core (Dahl-Jensen et al., 1993),

$$\Psi_{PP}(t) = \exp[\psi \Delta T_{TS}(t)], \tag{6}$$

with $\psi = 0.169/2.4 = 0.0704$ (Huybrechts, 2002). This simple relationship likely does not reflect the complexity of atmospheric circulation changes that governed moisture availability over the Alps during the last glacial cycle, of which little is known apart from the LGM (cf. Wu et al., 2007; Strandberg et al., 2011; Ludwig et al., 2016). Thus, another set of simulations presented here use constant precipitation, corresponding to $\psi = 0$.

3.3 Sensitivity of ice volume evolution

For the three palaeo-temperature records and the two palaeo-precipitation parametrizations used, the model yields significant ice volume build-up during MIS 4 and 2 (Fig. 2b), corresponding to documented glaciation periods in the Alps (Preusser, 2004; Ivy-Ochs et al., 2008). All simulations also yield important glaciations during MIS 5 and 3, but their timing and amplitude varies significantly depending on the climate forcing used. All six simulations overestimate the late-glacial re-advance during the Younger Dryas (12.9–11.7 ka; cf. e.g., Ivy-Ochs et al., 2009). This is partly because the 2 km resolution used in these simulations is too coarse to resolve Younger Dryas Alpine glaciers. However, the large total ice volume overestimation resulting from the GRIP temperature forcing (Fig. 2b, blue curves) certainly indicates that the vigorous cooling experienced during the Younger Dryas in Greenland is not representative of the Alps.

Geological data from the best documented Alpine piedmont lobes indicate that their maximum extension during MIS 2 occurred at around 25.5–24.0 ka (Monegato et al., 2017), after which Alpine glaciers remained or potentially re-advanced to within close reach of this maximum extent, until as late as 22 to 17 ka (Ivy-Ochs, 2015; Wirsig et al., 2016, Fig. 5). This is in very good agreement with the result of the EPICA simulations, which yield an early maximum ice volume at 25.2/24.6 (without/with palaeo-precipitation reductions) followed by a standstill until 17.3 ka (Fig. 2b, blue curves). The GRIP palaeo-temperature forcing, on the other hand, yields two distinct total ice volume maxima at 27.3/27.0 and 21.8/21.7 ka followed
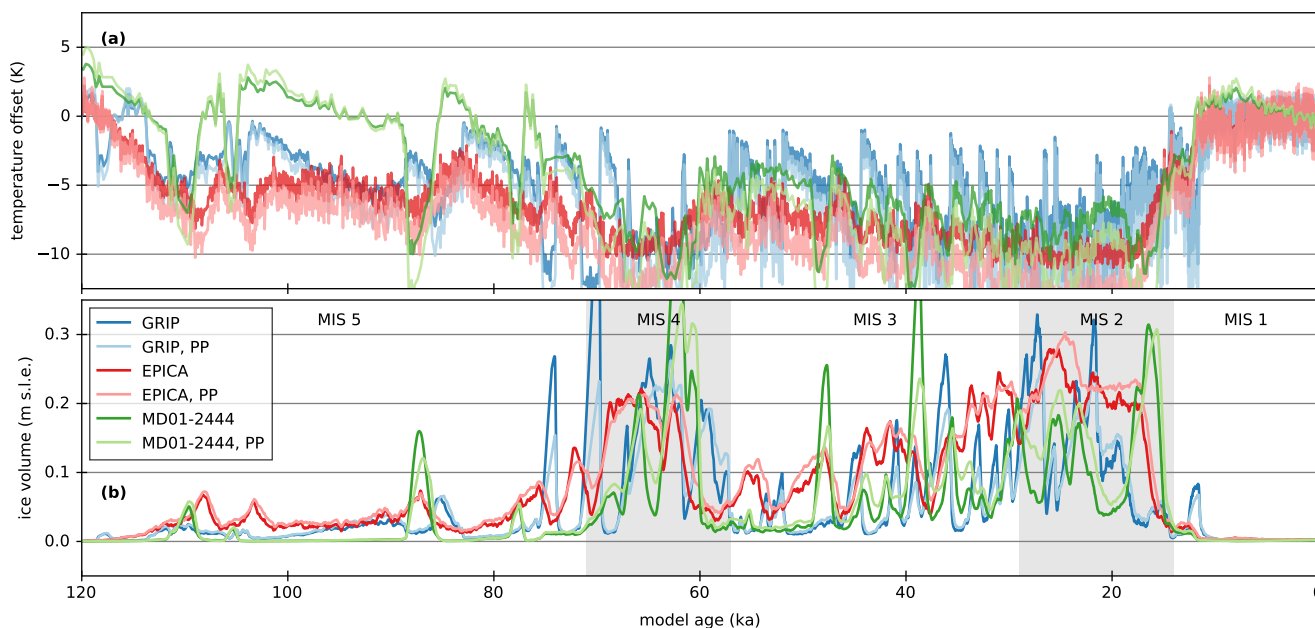
Figure 2. (a) Temperature offset time-series from ice core and ocean records (Table 2) used as palaeo-climate forcing for the ice sheet model. **(b)** Modelled total ice volume through the last 120 thousand years (ka) expressed in meters of sea-level equivalent (m s.l.e.). Gray fields indicate Marine Oxygen Isotope Stage (MIS) boundaries for MIS 2 and MIS 4 according to a global compilation of benthic δ^{18}O records (Lisiecki and Raymo, 2005). The simulation driven by the EPICA temperature yields smaller ice volume variability and a more realistic timing of deglaciation.

by an early deglaciation of the foreland by 21.4 ka. The MD01-2444 palaeo-temperature forcing yields a late LGM peak ice volume at 16.5/15.7 ka several thousand years after the dated geological evidence.

   Finally, all simulations yield very strong ice volume variability, indicative of many more than two or three cycles of glacier advance and retreats onto the foreland (Fig. 2b). Palaeo-precipitation reductions dampen some of the small-scale variability,

5 but they have little effect on the millennial scales that characterise those cycles (Fig. 2b, light colour curves). In particular, strong millennial variability recorded in GRIP δ^{18}O (Dansgaard-Oeschger events) have large repercussions on the modelled Alpine ice volume, including around six glaciations of LGM magnitude (Fig. 2b, blue curves), which is not supported by geologic evidence (Preusser, 2004; Ivy-Ochs et al., 2008). Dansgaard-Oeschger events, however, have been recorded in Central European lake sediments (Wohlfarth et al., 2008) and cave speleothems (Spötl and Mangini, 2002; Luetscher et al., 2015). Our

10 results indicate that their magnitude in Central Europe was likely lower than that recorded in GRIP δ^{18}O, which either implies smaller associated palaeo-temperature fluctuations in Central Europe than Greenland, or temperature-independent controls on GRIP δ^{18}O. In contrast, the EPICA palaeo-temperature record has least variability among the records used (Fig. 2a, red curves). This results in smaller variability in the total ice volume, and more restrictive glaciations during MIS 5 and 3, (Fig. 2b, red curves).
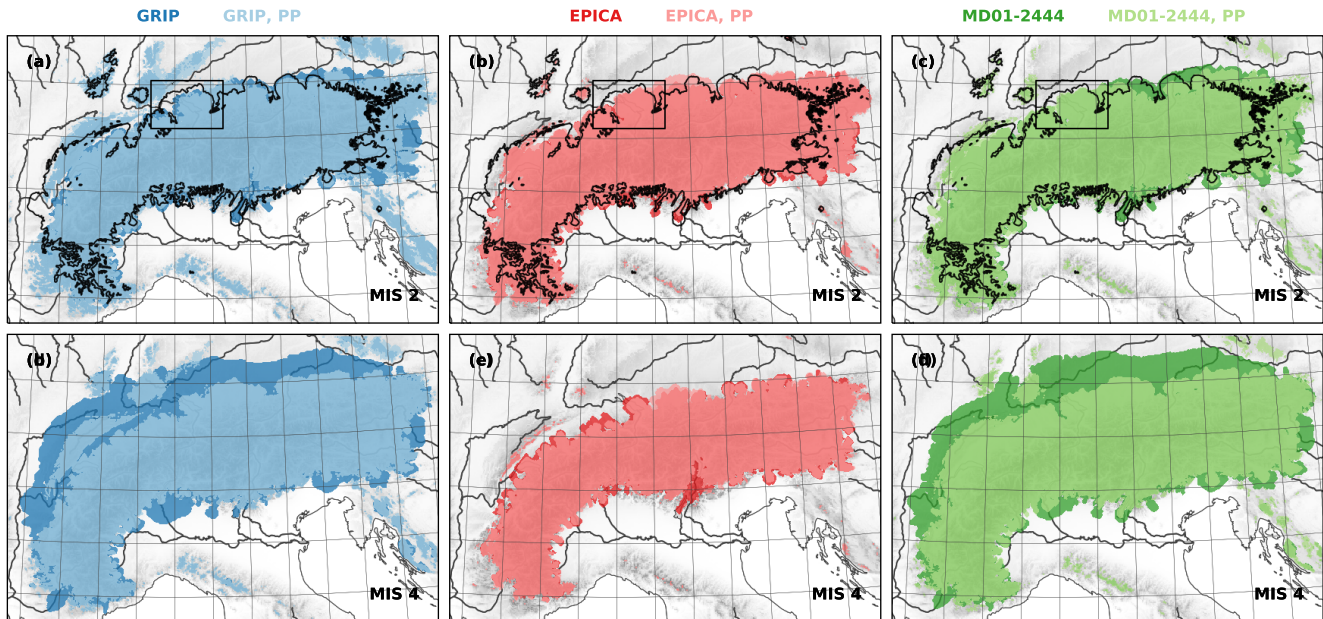
Figure 3. (a–c) Cumulative extent of modelled ice cover during MIS 2 (29–14 ka), without (dark colours) and with (light colours) palaeo-precipitation corrections, and using temperature time-series scaling factors (Table 2) adjusted to model the area glaciated by the Rhine glacier piedmont lobe (black rectangle) in agreement with the Last Glacial Maximum (LGM) geomorphological reconstruction (solid red line, Ehlers et al., 2011). **(d–f)** Cumulative extent of modelled ice cover during MIS 4 (71–57 ka). Only the simulation driven by the EPICA temperature time-series yields reasonable MIS 4 ice cover.

3.4 Sensitivity of glaciated area

During MIS 2, all six simulations yield comparative cumulative glaciated areas (Fig. 3a). This result is inherent to the palaeo-climate forcing approach used, which involves a linear scaling of each palaeo-temperature anomaly record to a geomorphological reconstruction of the area glaciated by the Rhine Glacier piedmont lobe (Sect. 3.1; Fig. 3a, black rectangle). Outside

5   this benchmark, all simulations underestimate glaciated area in the western part of the model domain, and overestimate it in the eastern part, relative to the geomorphological ice limits (Fig. 3a). This result might indicate that the LGM temperature depression, here taken as homogeneous, was actually lower in the Eastern Alps than in the Western Alps, as previously shown by positive degree-day modelling of the central European palaeo-ice caps (Heyman et al., 2013). Alternatively, the east-west gradient in winter precipitation existing today (Fig. 1h) was perhaps enhanced during the LGM, as indicated by pollen recon-

10   structions (Wu et al., 2007). Finally, the LGM extent of Alpine glaciers might have been affected by an east-west gradient in variables not accounted for by the PDD model, such as cloud cover or dust deposition.

Besides this general pattern, there exist differences in glaciated area depending on the palaeo-climate forcing used. The MD01-2444, and to a greater extent, the GRIP palaeo-temperature records, tend to overestimate MIS 2 ice cover on all pe-

ripheral ranges that surround the Alps (Fig. 3a and c). This is particularly true when no precipitation corrections are applied (bright colours). In fact, both palaeo-temperature records have a higher temperature variability and contain brief spells of cold temperatures, which are too short to develop a fully grown Alpine ice sheet, but long enough to build up ice cover on a smaller scale on these peripheral ranges (Fig. 2). On the other hand, peripheral glaciation modelled using the EPICA record (Fig. 3b),

5   which has smaller temperature variability, is in relatively good agreement with the geomorphological reconstructions.

The modelled extent of glaciation during MIS 4 depicts a more pronounced sensitivity to the choice of palaeo-climate forcing used. Using the GRIP and MD01-2444 palaeo-temperature records, Alpine glaciers are modelled to extend well beyond the reach of documented LGM end-moraines (Fig. 3d and f). Because, in both cases, the modelled glaciation extent corresponds to brief cold spells in the palaeo-temperature forcing (Fig. 2a), palaeo-precipitation reductions greatly reduce the excessive

10   modelled ice cover (Figs. 2b and 3d and f, light colours). However, with or without palaeo-precipitation corrections, the GRIP and MD01-2444 forcing yield modelled ice extents (Fig. 3d and f) and volumes (Fig. 2b) considerably larger during MIS 4 than during MIS 2, which is not supported by geological evidence (Preusser, 2004; Ivy-Ochs et al., 2008; Husen and Reitner, 2011; Barrett et al., 2017; Haldimann et al., 2017). Gravel deposits from the Rhine Glacier indicate an early last glacial cycle foreland glaciation, but the extent reached is less than that in MIS 2 (Keller and Krayss, 2010). Dropstones in lake sediments

15   indicate a late MIS 4 advance restricted to the upper Inn Valley (Barrett et al., 2017). For the Linth Glacier, no evidence for a pre-LGM glacier advance during the last glacial cycle is available (Haldimann et al., 2017).

The EPICA palaeo-temperature forcing, on the other hand, yields a MIS 4 glaciation that is only slightly less expansive than the MIS 2 glaciation (Fig. 3e). The sensitivity of the glaciated area to palaeo-precipitation reductions is mostly limited to the southern terminal lobes of central-Alpine glaciers, where reduced precipitation results in a slightly lesser extent during both

20   MIS 2 and 4 (Fig. 3b and e).

Based on the above considerations on timing of the LGM during MIS 2, and modelled ice extent during MIS 4, we select EPICA as our optimal palaeo-temperature record for a more detailed and higher-resolution comparison of modelled glacier dynamics to available geological evidence (Sect. 4). As a conservative approach in regard to the rapid ice volume fluctuations, we choose to include palaeo-precipitation corrections in the following higher-resolution run.

25   ## 4   Results and discussion

In this section, we compare the model output to geological evidence from the last glacial cycle, in terms of Last Glacial Maximum extent (Sect. 4.1), ice flow patterns (Sect. 4.2), timing of the Last Glacial Maximum (Sect. 4.3), ice thickness (Sect. 4.4), and glacial cycle dynamics (Sect. 4.5).

This simulation is forced by the optimal EPICA palaeo-temperature record (Sect. 3.1) and includes palaeo-precipitation

30   reductions (Sect. 3.2). It uses a horizontal resolution of 1 km. The vertical grid consists of 61 temperature layers in the bedrock and up to 251 enthalpy layers in the ice, corresponding to vertical resolutions of 50 and 20 m, respectively. This simulation ran for 33 days using 576 processors.
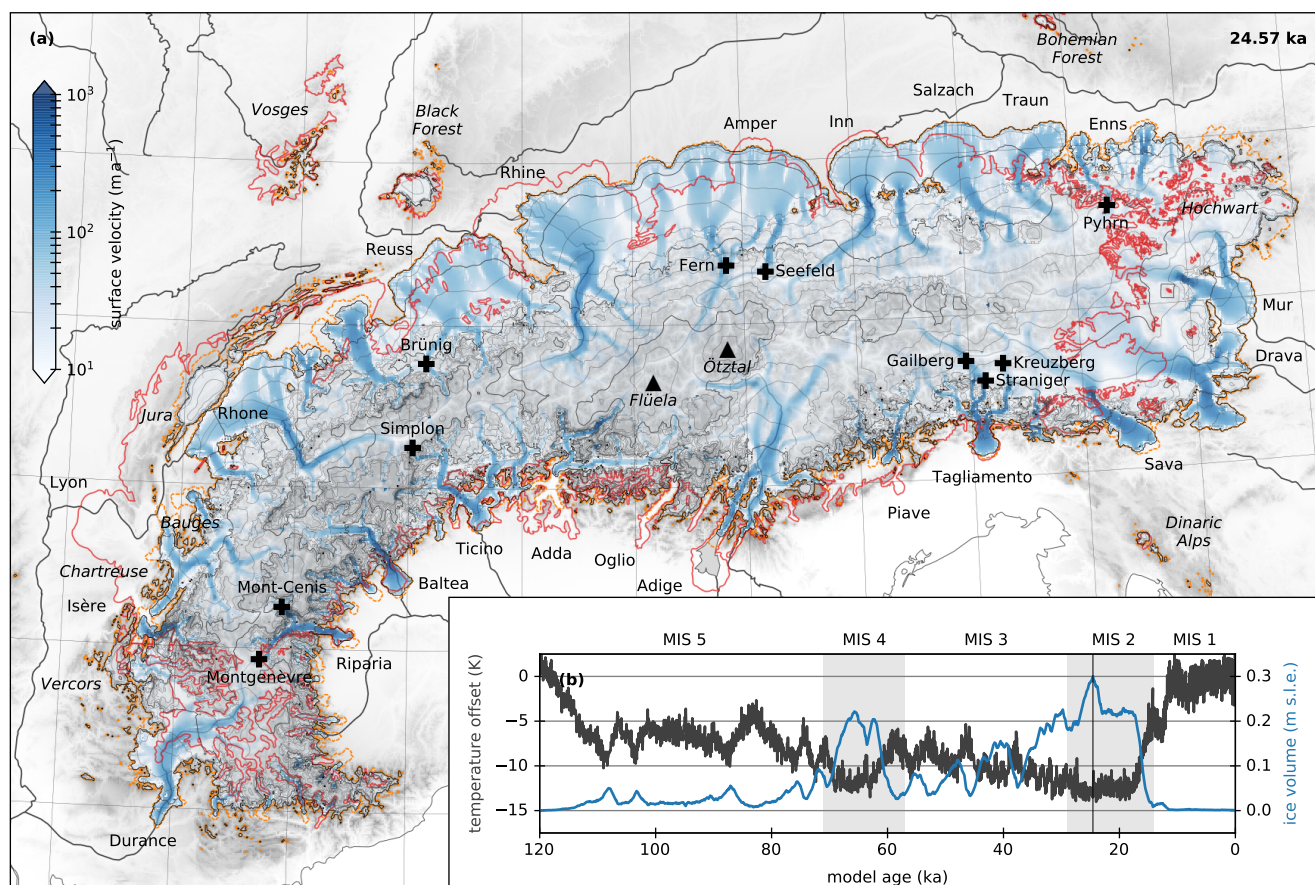
Figure 4. (a) Modelled bedrock topography (grey), ice surface topography (200 m contours), and ice surface velocity (blue) in the Alps 24.57 ka before present, corresponding to the maximum modelled ice cover. Modelled self-sustained ice domes (triangles) and some major transfluences (crosses) are shown. Modelled LGM ice extent (dashed orange line) and geomorphological reconstruction (solid red line, Ehlers et al., 2011). The background map consists of depressed SRTM (Jarvis et al., 2008) topography and Natural Earth Data (Patterson and Kelso, 2017). (b) Temperature offset time-series from the EPICA ice core used as palaeo-climate forcing for the ice flow model (black curve, Jouzel et al., 2007), and modelled total ice volume through the last glacial cycle (120–0 ka), expressed in meters of sea level equivalent (m s.l.e., blue curve). Gray fields indicate Marine Oxygen Isotope Stage (MIS) boundaries for MIS 2 and MIS 4 according to a global compilation of benthic δ^{18}O records (Lisiecki and Raymo, 2005).

4.1 Last Glacial Maximum ice extent

The LGM extent of Alpine glaciers has been mapped with varying level of detail across the Western (Coutterand, 2010; Buoncristiani and Campy, 2011; Jäckli, 1962; Bini et al., 2009; Hantke, 2011), and Eastern Alps (Penck and Brückner, 1909; Castiglioni, 1940; van Husen, 1987; BGR, 2007; van Husen, 2011; Bavec and Verbič, 2011). Some of these maps have been

compiled into a reconstruction, covering the entire Alps (Ehlers et al., 2011), and reproduced here (Fig. 4, red line) for com-
parison against model results.

The modelled total ice volume reaches a maximum of 123×10^3 km^3, or 300 mm of sea-level equivalent, at 24.56 ka (Fig. 4b).
A maximum glacierized area of 163×10^3 km^2 is attained shortly afterwards at 24.57 ka (Fig. 4a). Although the modelled timing
5 of the LGM varies accross the mountain range (Sect. 4.3), at 24.57 ka nearly all outlet glaciers extend to within a few kilometres
from their modelled maximum stage (Fig. 4a, dashed orange line).

The palaeo-climate forcing was adapted (Sect. 3.1) to model the maximum configuration of the Rhine Glacier in broad
agreement with the geological reconstruction of the LGM extent (Fig. 4a, solid red line), yet discrepancies remain elsewhere.
As already outlined for low resolution runs (Sect. 3.4), the extent of glaciation in the north-western Alps, including the Rhone
10 Glacier complex, the Jura ice cap, and the Lyon Lobe, is underestimated in the model results (Fig. 4a, cf Bini et al., 2009;
Coutterand, 2010). On the other hand, the model yields excessive ice cover in the eastern Alps, where the Mur, Drava and Sava
Glaciers are modelled to extend tens of km beyond the mapped ice limits (Fig. 4a, cf van Husen, 1987; Bavec and Verbič,
2011). As previously discussed, these discrepancies might indicate that the LGM climate was characterized by an east-west
gradient in temperature (cf. Heyman et al., 2013) or precipitation (cf. Wu et al., 2007) anomalies relative to present, or an
15 east-west gradient in variables that are not accounted for by the PDD model.

On the other hand, while atmospheric circulation models (Strandberg et al., 2011; Ludwig et al., 2016) and palaeo-climate
proxies (Luetscher et al., 2015) both support differential precipitation changes north and south of the Alps, our model results
show no obvious north-south bias as compared to the mapped LGM margins (Fig. 4a) despite the homogeneous temperature
and precipitation anomalies applied relative to present. Although this may appear as a contradiction with previous, constant-
20 climate modelling results (Becker et al., 2016), it follows from introducing a time-dependent palaeo-temperature forcing.
Without introducing differential precipitation change north and south of the Alps, constant climate forcing systematically
resulted in extraneous (Becker et al., 2016, Fig. 3) and premature (Becker et al., 2016, Fig. 4) glaciation on the north slope
of the Alps. Using time-dependent palaeo-temperature forcing, progressive atmospheric cooling over several thousand years
allow for warmer temperatures, closer to the thermodynamic equilibrium, within the ice and the bedrock. This results in thinner
25 glaciers and limits overshoot of the equilibrium state (discussed further in Sect. 4.3).

On a more regional level, the maximum extent of the Ticino, Oglio, Adige and Piave Glaciers in the central southern Alps is
modelled several kilometres within the mapped LGM moraines (Fig. 4a). This appears to result from the palaeo-precipitation
reduction used to force the model (Fig. 3b), which is likely unrealistic in at least this part of the model domain. On the
other hand, the Durance glacier in the south-western Alps is modelled to extend several kilometers beyond the mapped limit
30 (Fig. 4a), indicating that the LGM temperature depression was likely dampened by Mediterranean climate in this part of the
model domain.

The model reproduces peripheral ice caps where documented by geological evidence on the Vercors, Chartreuse and Bauge
Prealpine reliefs, the Jura Mountains, the Vosges Mountains, the Black Forest, the Bohemian Forest and the Dinaric Alps
(Fig. 4a). An independent ice cap also covers the Hochwart massif during most of the simulation, yet it is engulfed by Alpine
35 glaciers during the LGM to become a peripheral ice dome (Fig. 4a; cf. van Husen, 2011, Fig. 2.5). The LGM extent of

peripheral ice caps is underestimated in the Vosges and Jura mountains, but it is overestimated for the more meridional Vercors Massif (Fig. 4a; cf. Coutterand, 2010, Figs. 4.28, 4.32, and 4.33, p. 322–321). Thus, there exists a regional conformity between the model-data discrepancies obtained for the main Alpine ice sheet and those obtained for peripheral ice caps, including too extensive modelled ice cover to the East and extreme South-West, and too restrictive modelled ice cover to the North-West.

5 Because peripheral ice caps have very different glacier dynamics than the main ice sheet, this conformity most likely indicates a climatic cause, rather than an ice dynamics cause, for these discrepancies.

4.2 Ice flow patterns

The LGM Alpine ice flow pattern was traditionally described as that of a network of interconnected valley glaciers, primarily controlled by subglacial topography. However, geomorphology shows that ice was thick enough to flow accross high mountain

10 passes throughout the mountain range (e.g., Onde, 1938; Penck and Brückner, 1909; Jäckli, 1962; van Husen, 1985, 2011; Kelly et al., 2004; Coutterand, 2010), and even perhaps to form self-sustained ice domes (Florineth, 1998; Florineth and Schlüchter, 1998; Kelly et al., 2004; Bini et al., 2009).

The modelled flow pattern at 24.57 ka is complex (Fig. 4a, blue colour mapping). Ice velocities of several hundred metres per year, characteristic for basal sliding, generally occur along the main river valleys, while ice domes and ice divides are predom-

15 inantly located over major reliefs areas, where ice moves only by a few metres per year, characteristic for internal deformation without basal sliding (Fig. 4a). Nevertheless, the model results depict exceptions to this general pattern as occasional ice flow across the modern water divides, i.e. transfluences.

In the Western Alps, major transfluences occur for instance across Col de Montgenèvre, Col du Mont-Cenis, Simplon Pass and Brünig Pass (Fig. 4a). Although a transfluence across Col de Montgenèvre was previously questioned (Cossart et al.,

20 2012, Fig. 2), evidence for southerly ice flow across Col du Mont-Cenis has been recognized (Onde, 1938; Coutterand, 2010, Fig. 3.18, p. 284). Similarly, tranfluences have been previously identified from the geomorphology across Simplon Pass (Kelly et al., 2004) and from the distribution of glacial erratics across Brünig Pass (Jäckli, 1962). On the other hand, the simplified climate forcing used in this sumulation could not reproduced the transport of glacial erratics from southern Valais to observed deposition sites in the Solothurn region (cf. Jouvet et al., 2017).

25 In the Eastern Alps, major transfluences are modelled to have occur for instance across Fern Pass, the Seefeld Saddle, the Gailberg Saddle, the Kreuxberg Saddle, the Straniger Alp, and Pyhrn Pass (Fig. 4a). Transfluences across Fern Pass and the Seefeld Saddle are known from the geomorphology (Penck and Brückner, 1909; van Husen, 2011, Fig. 2.4). It is also known that ice flowed across the Gailberg and Kreuzberg saddles (van Husen, 1985), and Pyhrn Pass (van Husen, 2011, Fig. 2.5). On the other hand, no transfluence has previously been documented at the Straniger Alp. The Tagliamento catchment is usually

30 assumed to not have received tranfluences from the Drava catchment (Monegato et al., 2007), but this would not be incompatible with reconstructed ice surface elevations in this area (van Husen, 1987).

Finally, self-sustained ice domes characteristic of ice caps are modelled in two locations over Flüela Pass and Ötztal (Fig. 4a). These modelled ice domes exhibit radial ice surface slopes and radial flow velocities crosscutting the underlying topographic troughs and ridges. On the one hand, ice-dispersal centres previously labelled as ice domes in the upper Rhone and Rhine
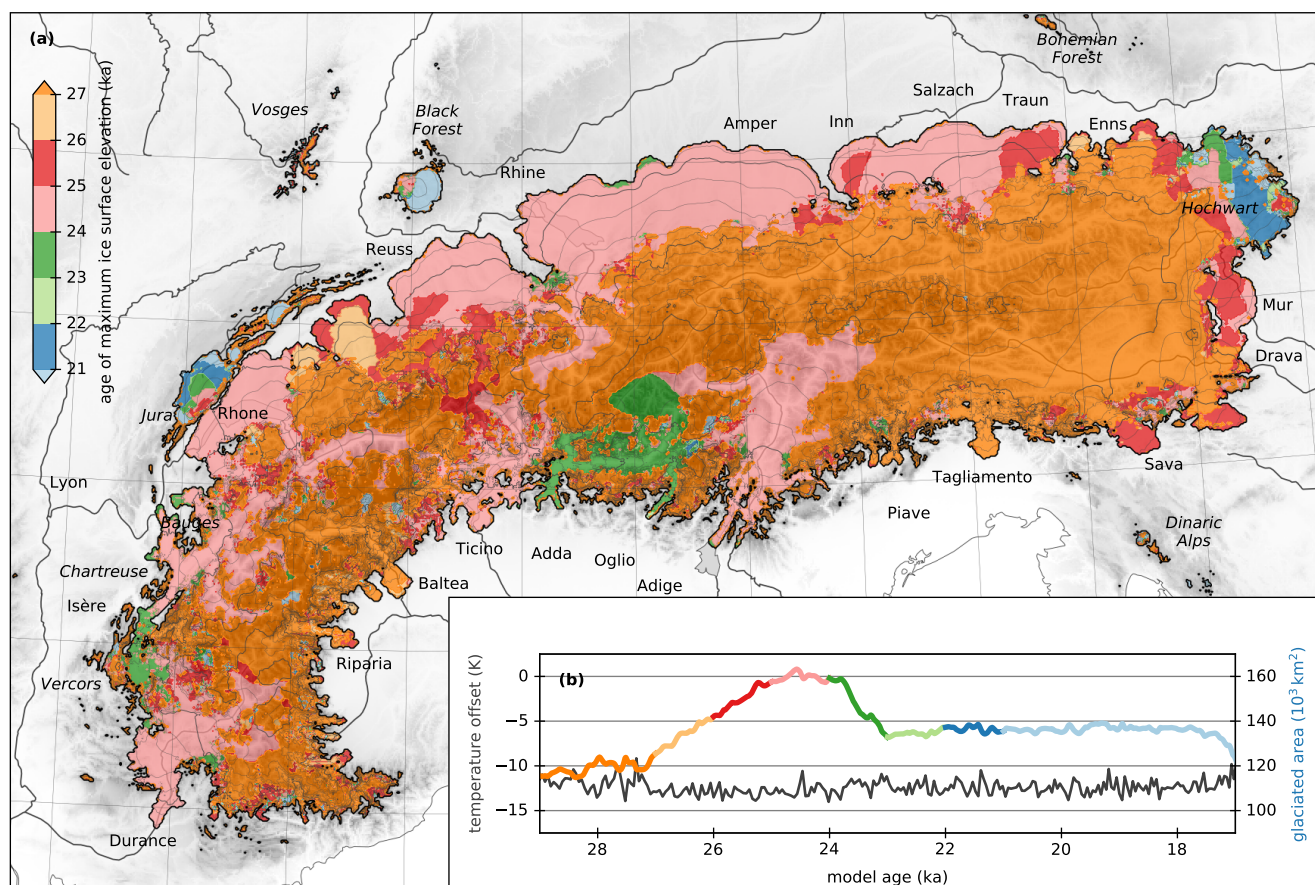
Figure 5. (a) Timing of the LGM given by the modelled age of maximum ice thickness throughout the entire simulation (colour mapping) and corresponding, ice surface elevation (200 m contours). **(b)** Temperature offset time-series from the EPICA ice core used as palaeo-climate forcing for the ice flow model (black curve), and modelled glacierized area during the LGM (coloured curve). The LGM is here modelled as a time-transgressive event.

Valley (Florineth and Schlüchter, 1998; Kelly et al., 2004; Bini et al., 2009) feature as mere ice divides in our simulation. On the other hand, the modelled ice dome over Flüela Pass overlaps with the previously mapped Engadine ice dome (Florineth, 1998), although its centre is modelled ca. 20 km north of that indicated by geomorphology (Florineth, 1998, Fig. 3).

Except for too extensive ice cover in the easternmost part of the model domain (Sect. 4.1), there is generally a good agreement between transfluences observed in the geomorphology and the model results. Both depict the LGM Alpine ice flow pattern as an intermediate between that of a topography-controlled ice field, and that of a self-sustained ice cap.

4.3 Timing of the Last Glacial Maximum

The timing of the LGM has been documented by radiocarbon and cosmogenic isotope dating techniques at multiple locations around the Alps (cf. Ivy-Ochs, 2015; Wirsig et al., 2016, Fig. 5 for reviews; and the more recent publications by Monegato et al., 2017; Federici et al., 2017). These data indicate that Alpine glaciers reached their maximum extent between 26 and 20 ka (calibrated ^{14}C and ^{10}Be ages), but also that terminal lobes stayed in the foreland until 22 ka to 17 ka, when they experienced rapid retreat synchronously to lowering of the ice surface in the mountains (Ivy-Ochs, 2015; Wirsig et al., 2016, Fig. 5; Monegato et al., 2017, Fig. 3).

In our simulation, the maximum areal cover is reached at 24.57 ka (Fig. 4a), yet individual glacier lobes reach their maximum extent at different ages (Fig. 5). For instance, the Dora Riparia, Dora Baltea, and Tagliamento Glaciers reach an early maximum before 27 ka; the Durance, Rhone, Inn, Enns, Ticino, and Adige Glaciers reach their maximum thickness in phase with the overall Alpine areal maximum around 25 ka; while the Isère, Adda and Oglio Glaciers reach a late maximum after 24 ka (Fig. 5). Remarkably, peripheral ice caps on the Vercors, Jura Mountains, Black Forest and Hochschwab reach their maximum extent even later and locally after 21 ka (Fig. 5).

These differences in timing of the LGM occur in the model results despite the homogeneous temperature and precipitation anomalies supplied as palaeo-climate forcing. The LGM timing differences modelled here are thus not related to climate, but are inherent to modelled glacier dynamics. They result from differences in the subglacial topography, in particular catchment sizes and hypsometry, of the different outlet glaciers.

For large Alpine glaciers flowing in deep valleys, such as the Rhone, Rhine and Adige Glaciers, several thousand model years are needed to attain a thermodynamical equilibrium between cold-ice advection from the high accumulation areas, upward diffusion of geothermal heat, and heat release from strong basal shear strain. Temperature evolution is, in part, limited by the slow warming of the subglacial bedrock, that has been previously cooled downed by subfreezing air temperature before glacier advance. For larger glaciers, this thermodynamical equilibrium is typically not yet attained around 25 ka. This is why several Alpine lobes overshoot their balanced extent before thinning and receding towards the mountains as they warm towards thermodynamical equilibrium (supplementary animation). In contrast, peripheral ice caps with basal topography restricted to high elevations experience very low shear strain and virtually no basal sliding. They advance regularly on a frozen bed during the entire cold period, resulting in a late maximum stage (Fig. 5).

Our results indicate that even for a relatively small ice sheet like that found in the Alps, the LGM glacier extent corresponds to a transient stage, while millennial-scale spatial differences in its timing can result not only from climate variability but also from complex glacier dynamics. Heterogeneous climatic anomalies, such as temperature or precipitation anomaly gradients, not included in our model set-up, have perhaps induced further spatial differences in the timing of the LGM Alpine ice sheet, which may have counterbalanced or enhanced those modelled here.
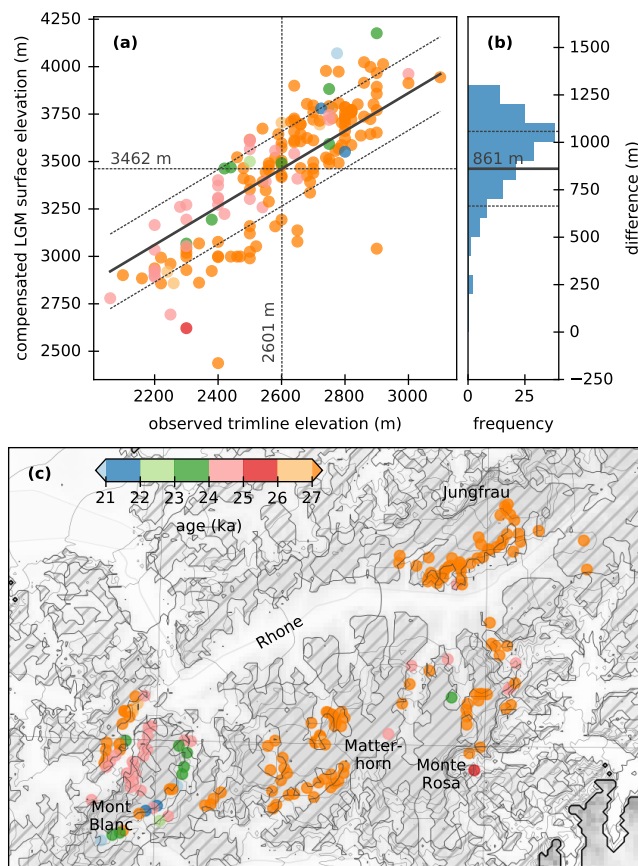
Figure 6. (a) Comparison of modelled ice surface elevation at the LGM (time-transgressive, corresponding to maximum ice thickness, Fig. 5), compensated for bedrock deformation, against observed trimline elevations for the upper Rhone Glacier (Kelly et al., 2004, Table 1). Colours show the age of maximum ice thickness (as in Fig. 5). Model variables were bilinearly interpolated to the trimline locations. **(b)** Histogram of differences between modelled LGM ice surface elevation and trimline elevations (50 m bands). The average difference is 861 m. **(c)** Observed upper Rhone Valley trimline locations (Kelly et al., 2004, Table 1), modelled age of maximum ice thickness (colour) and LGM ice surface elevation (200 m contours). Hatches mark areas modelled to have been glaciated but to have experienced temperate ice for less than 1 ka during MIS 2 (29–14 ka).

4.4 Ice thickness and trimlines

Following the general assumption that trimlines, which mark the transition between the steep frost-shattered ridges and the more gentle glacially sculpted valley troughs, represent the maximum elevation of the LGM ice surface, maximum ice thickness in the Alps has been reconstructed in several areas (van Husen, 1987; Florineth, 1998; Florineth and Schlüchter, 1998; Kelly et al., 2004; Bini et al., 2009; Coutterand, 2010; Cossart et al., 2012). However, this assumption is challenged by geomorphological and cosmogenic nuclide dating evidence from Scandinavia (e.g., Kleman, 1994; Kleman and Borgström, 1994), the

British Isles (e.g., Fabel et al., 2012), and North America (e.g., Kleman et al., 2010), that pre-glacial landscapes located well above the trimlines have been glaciated and preserved under cold-based ice, sometimes for several glacial cycles (Stroeven et al., 2002). Thus, the trimline could also mark the maximum elevation of the transition from temperate to cold-based ice, or a late-glacial ice surface elevation (Coutterand, 2010, Fig. 1, p. 403). However, no such evidence has been reported in the Alps.

5   In the upper Rhone Valley, the maximum ice surface elevation reached during MIS 2 in our simulation, corrected for bedrock deformation, is consistently modelled to have occured several hundred metres above the observed trimline elevations (Fig. 6a and b), with a mean difference of 861 m (Fig. 6b), wich is significant in respect to the modelled regional ice thickness. The result is somewhat dependent on uncertain basal sliding and ice rheological parameters to which the model sensitivity was not tested here. However, a previous sensitivity study conducted with PISM and a very similar model set-up on the Cordilleran ice

10   sheet show that varying ice rheological parameters resulted in relative errors in modelled total ice volume of 25 % with regard to ice rheological parameters and 14 % regarding basal sliding parameters (Seguinot et al., 2016, Fig. 7). In addition, regional sensitivity tests in the Rhone Valley show that a modelled ice surface compatible with the trimline elevations is incompatible with the documented overspilling flow to the south across the Simplon pass (Becker et al., 2017).

      Our model results depict a polythermal LGM Alpine ice cover. Due to sub-freezing temperatures applied in the climate

15   forcing of the model, the entire Alpine ice sheet is capped by an upper layer of cold ice. In major Alpine valleys, such as the upper Rhone Valley, important ice thickness and strain heating contribute to form a layer of temperate ice near the glacier base, allowing basal melt, sliding and potentially erosion (Fig. 6c, white areas). On the other hand, on the highest mountains, ice cover is too thin and too static to form temperate ice, resulting in cold ice down to the bed and preventing potential erosion (Fig. 6c, hatched areas).

20   In the upper Rhone Valley, the geographical location of observed trimlines show a remarkable agreement with the areal extent of regions that are modelled to have experienced warm-based ice for less than 1 ka (7 %) of the MIS 2 (Fig. 6c). Although this result calls for more detailed comparisons across the entire Alpine range and specific sensitivity studies to relevant basal sliding and ice rheological parameters, and to the uncertain subglacial topography the presence of an upper layer of cold ice during the LGM, already found at high altitude in the much warmer climate of today (e.g., Suter et al., 2001; Bohleber et al., 2017),

25   is inevitable (Haeberli and Schlüchter, 1987, Fig. 3). In this context, our results challenge the assumption that Alpine trimlines mark the maximum upper ice surface elevation of the LGM ice cover and call for a more accurate estimation of the thickness of the upper layer of cold ice in the Alps.

4.5   Glacial cycle dynamics

Glacial history of the Alps prior to the LGM remains poorly constrained. Although the four glaciations model (Penck and

30   Brückner, 1909) has long been used, it is now known that glaciers advanced onto the foreland at least 15 times since the beginning of the Quaternary at 2.58 Ma (Schlüchter, 1991; Preusser et al., 2011). Sparse geological data indicate that the last glacial cycle may have comprised two or even three periods of glacier growth and decay (Preusser, 2004; Ivy-Ochs et al., 2008). Luminescence dating from two sites in the central northern foreland indicate an early last glacial advance of Alpine glaciers onto the near foreland around 107 ± 9 to 101 ± 5 ka (Preusser et al., 2003; Preusser and Schlüchter, 2004). Evidence
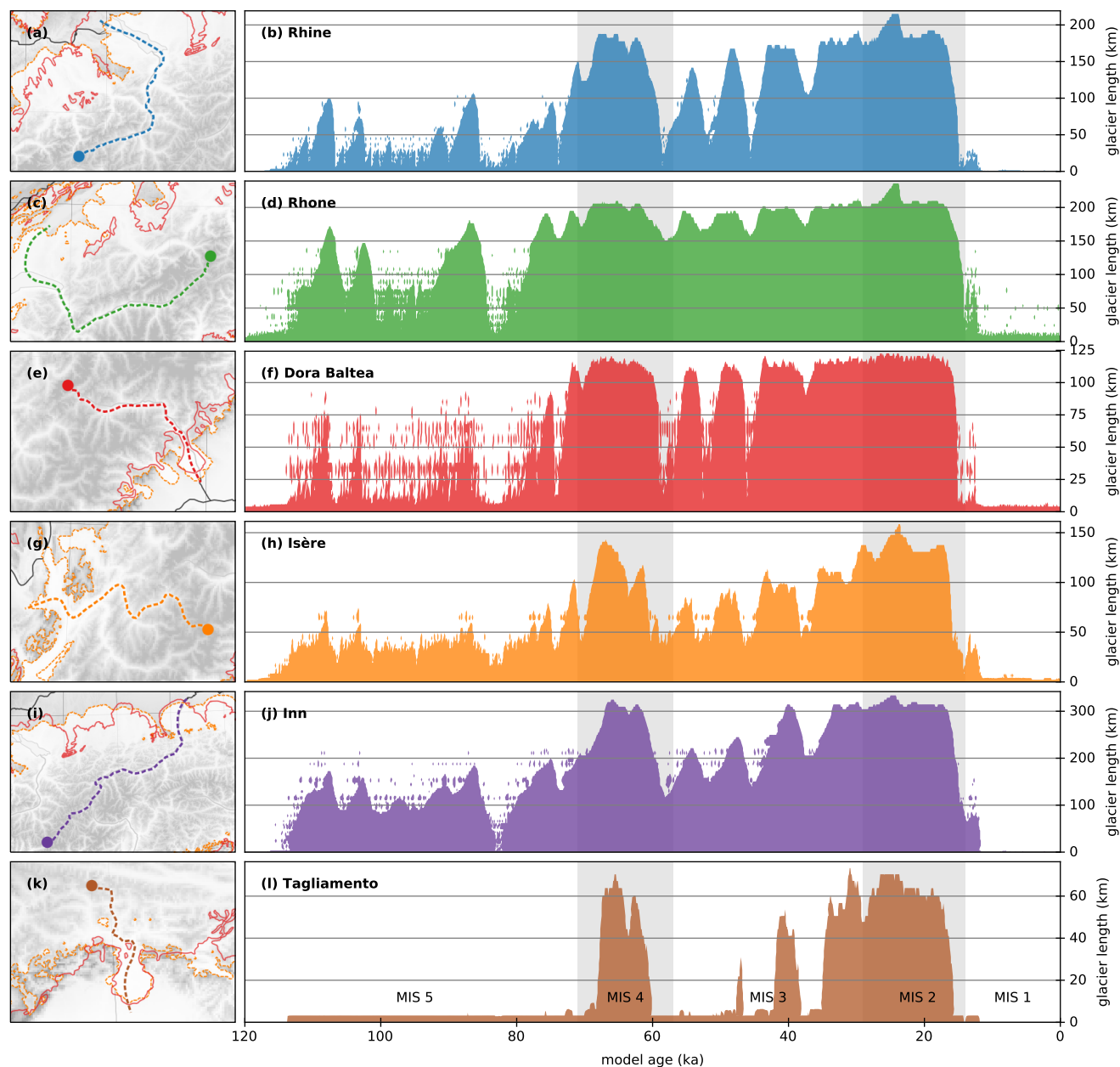
Figure 7. (a, c, e, g, i, k) Profile lines roughly following valley centerlines for the Rhine, Rhone, Dora Baltea and Isère, Inn and Tagliamento Glaciers. **(b, d, f, h, j, l)** Evolution of modelled glacier extent in time, bilinearly interpolated along the corresponding profiles, showing numerous cycles of advance and retreat over the last glacial cycle modulated by subglacial topography and catchment geometry. Isolated patches indicate periodic surges from tributary glaciers.

for a MIS 4 glaciation is equally sparse (Sect. 3.4; Keller and Krayss, 2010; Barrett et al., 2017; Haldimann et al., 2017), and its timing remains uncertain (e.g., Link and Preusser, 2006; Preusser et al., 2007).

As previously mentioned (Sect. 3.3), independent of the palaeo-temperature (GRIP, EPICA, or MD01-2444) and palaeo-precipitation (with or without corrections) applied, all simulations presented here result in a high temporal variability in the

5   total modelled ice volume (Fig. 2). Using the optimal EPICA palaeo-temperature record with least variability (Sect. 3.1) and conservatively including palaeo-precipitation reductions (Sect. 3.2), the 1 km resolution simulation also results in strong total ice volume variability throughout the last glacial cycle (Fig. 4b). Two major glaciations occur during MIS 4 and 2 (Fig. 4b). However, several minor glaciations occur during MIS 5 and 3, as well as a minor late-glacial readvance at the onset of MIS 1 (Fig. 4b). These episodes are the result of synchronous advances of several Alpine glaciers well into the major valleys and

10   sometimes even onto the foreland (Fig. 7; supplementary animation).

For instance the Rhine Glacier (Fig. 7a) reaches a length exceeding 130 km, roughly corresponding to the location of the last major Alpine reliefs and the beginning of the foothills, six times during the simulation, and sometimes retreats almost completely between two advances (Fig. 7b). The Rhone Glacier, fed by several high-altitude accumulation areas, advanced eight times onto modern Lake Geneva (Fig. 7c and d). The Dora Baltea Glacier, characterised by a very steep catchment,

15   and mutliple tributaries, shows even a higher variability and reaches close to its maximum position six times throughout the simulation (Fig. 7e and f). The Isère (Fig. 7g and h) and Inn (Fig. 7i and j) Glaciers, with their complex system of confluences and diffluences, need longer time to build up and reach the foreland only two or three times (Fig. 7g–j). Finally, the Tagliamento Glacier, distant from the major ice-dispersal centres of the inner Alps, is absent for most of the modelled glacial cycle (Fig. 7k and l)

20   Despite the low temperature variability of the palaeo-climate forcing, and reduced precipitation dampening glacier response, our simulation depicts the Alpine ice complex as highly dynamic, with many more than two or three (cf. Preusser, 2004; Ivy-Ochs et al., 2008) glaciations, and regional glacier dynamics controlled by spatial variations in catchment size and hypsometry. Importantly, Dansgaard-Oeschger events, recorded in Central Europe (Spötl and Mangini, 2002; Wohlfarth et al., 2008; Luetscher et al., 2015) but absent from the EPICA palaeo-temperature forcing, may have induced an even more dynamic

25   glacier response than that modelled here.

5   Conclusions

This study consists in the application of the numerical ice sheet model PISM to ice dynamics of the last glacial cycle in the Alps, using a model set-up based on that previously developed and validated for the Cordilleran ice sheet (Sect. 2). Using three different palaeo-temperature forcing records (GRIP, EPICA, and MD01-2444; Sect. 3.1), scaled to reproduce the Rhine Glacier

30   piedmont lobe in agreement with the mapped LGM ice margin, and two different palaeo-precipitation parametrizations (with and without precipitation reductions; Sect. 3.2), we find that only the EPICA palaeo-temperature record yields model results in agreement with geological findings, in the sense that:

- The EPICA palaeo-temperature forcing yields maximum ice volume at 25.2/24.6 ka (without/with palaeo-precipitation reduction), followed by a standstill of major piedmont lobes in the forelands until 17.3 ka, both compatible with much of the dating results, whereas the GRIP forcing results in early deglaciation of the foreland complete by 21.4 ka, and the MD01-2444 forcing results in a late LGM glaciation peaking at 16.5/15.7 ka (Sect. 3.3).

5
- The EPICA palaeo-temperature forcing yields cumulative ice extent compatible with geological evidence during MIS 4 and 2, whereas both GRIP and MD01-2444 forcing result in MIS 4 glaciation well beyond the mapped LGM ice limits (Sect. 3.4).

We then use this optimal palaeo-temperature forcing and, as a conservative approach, palaeo-precipitation reductions, to force a 1-km resolution simulation of the last glacial cycle in the Alps. A more detailed analysis of its output lead us to the
10 following conclusions.

- Ice cover is generally underestimated in the north-western Alps and overestimated in the eastern and south-western Alps, indicating that east-west gradients in temperature or precipitation change, absent from our model forcing, probably controlled the LGM extent of ice cover in the Alps. The asymmetric extent north and south of the Alps can be explained by the transient nature of the LGM extent without involving north-south gradients in temperature and precipitation
15 change (Sect. 4.1).

- The LGM ice flow pattern in the Alps was largely controlled by subglacial topography, but several transfluences and two self-sustained ice domes may have occurred (Sect. 4.2).

- The LGM (maximum) extent was a transient stage in which glaciers were out of balance with the contemporary climate. Its timing potentially varied across the range due to inherent glacier dynamics (Sect. 4.3).

20
- Ice thickness during the LGM is modelled to be much higher than in reconstructions. In average, modelled surface elevation is 861 m above the Rhone Glacier trimlines, which may instead indicate an englacial thermal boundary (Sect. 4.4).

- Alpine glaciers were potentially very dynamic. They quickly responded to climate fluctuations and some potentially advanced many times over the foreland during the last glacial cycle (Sect. 4.5).

These results are nevertheless limited by the simplicity of the climate forcing and surface mass balance model applied, and
25 uncertainties in ice flow physics. In particular, additional palaeo-climate variability over the European Alps may have caused more glaciations than modelled here. Through more detailed sensitivity studies, targeted to specific aspects of the last glacial cycle ice dynamics in the Alps, future modelling studies will certainly be able to quantify uncertainties associated with some of the above statements. Nevertheless, we hope that these conclusions will also serve as a basis for future studies of glacial geology in the Alps, and call for a more systematic aggregation and homogenization of glacial geological data to form a basis
30 for model validation across the entire Alpine range.

Code and data availability. PISM is available as open-source software at http://pism-docs.org/. Upon publication, we will be happy to make aggregated model output available through The Cryosphere. Please contact the corresponding author for mode detailed model output data.

Author contributions. J. Seguinot designed the study, ran the simulations, and wrote most of the manuscript. M. Huss provided modern ice thickness data. All authors contributed to interpreting results and improving the text. The idea for this study stems in part from an excursion
5 organised by F. Preusser in the central Alps in 2012.

Competing interests. We have no conflict of interest in publishing these results.

References

Agassiz, L.: Etudes sur les glaciers, Jent et Gassmann, Soleure, 1840.

Aschwanden, A., Bueler, E., Khroulev, C., and Blatter, H.: An enthalpy formulation for glaciers and ice sheets, J. Glaciol., 58, 441–457, https://doi.org/10.3189/2012JoG11J088, 2012.

5 Aschwanden, A., Aðalgeirsdóttir, G., and Khroulev, C.: Hindcasting to measure ice sheet model sensitivity to initial states, The Cryosphere, 7, 1083–1093, https://doi.org/10.5194/tc-7-1083-2013, 2013.

Augustin, L., Barbante, C., Barnes, P. R. F., Barnola, J. M., Bigler, M., Castellano, E., Cattani, O., Chappellaz, J., Dahl-Jensen, D., Delmonte, B., Dreyfus, G., Durand, G., Falourd, S., Fischer, H., Flückiger, J., Hansson, M. E., Huybrechts, P., Jugie, G., Johnsen, S. J., Jouzel, J., Kaufmann, P., Kipfstuhl, J., Lambert, F., Lipenkov, V. Y., Littot, G. C., Longinelli, A., Lorrain, R., Maggi, V., Masson-Delmotte, V.,
10 Miller, H., Mulvaney, R., Oerlemans, J., Oerter, H., Orombelli, G., Parrenin, F., Peel, D. A., Petit, J.-R., Raynaud, D., Ritz, C., Ruth, U., Schwander, J., Siegenthaler, U., Souchez, R., Stauffer, B., Steffensen, J. P., Stenni, B., Stocker, T. F., Tabacco, I. E., Udisti, R., van de Wal, R. S. W., van den Broeke, M., Weiss, J., Wilhelms, F., Winther, J.-G., Wolff, E. W., and Zucchelli, M.: Eight glacial cycles from an Antarctic ice core, Nature, 429, 623–628, https://doi.org/10.1038/nature02599, 2004.

Barrett, S., Starnberger, R., Tjallingii, R., Brauer, A., and Spötl, C.: The sedimentary history of the inner-alpine Inn Valley, Austria: extending
15 the Baumkirchen type section further back in time with new drilling, J. Quaternary Sci., 32, 63–79, https://doi.org/10.1002/jqs.2924, 2017.

Bavec, M. and Verbič, T.: Glacial History of Slovenia, in: Ehlers et al. (2011), pp. 385–392, https://doi.org/10.1016/b978-0-444-53447-7.00029-5, 2011.

Becker, P., Seguinot, J., Jouvet, G., and Funk, M.: Last Glacial Maximum precipitation pattern in the Alps inferred from glacier modelling, Geographica Helvetica, 71, 173–187, https://doi.org/10.5194/gh-71-173-2016, 2016.

20 Becker, P., Funk, M., Schlüchter, C., and Hutter, K.: A study of the Würm glaciation focused on the Valais region (Alps), Geographica Helvetica, 72, 421–442, https://doi.org/10.5194/gh-72-421-2017, 2017.

BGR: Geologische Übersichtskarte der Bundesrepublik Deutschland 1:200,000, Bundesanstalt für Geowissenschaften und Rohstoffe, Hannover, various sheets, 2007.

Bini, A., Buoncristiani, J.-F., Couterrand, S., Ellwanger, D., Felber, M., Florineth, D., Graf, H. R., Keller, O., Kelly, M., Schlüchter, C., and
25 Schoeneich, P.: Die Schweiz während des letzteiszeitlichen Maximums (LGM), Bundesamt für Landestopografie swisstopo, 2009.

Bohleber, P., Hoffmann, H., Kerch, J., Sold, L., and Fischer, A.: Investigating cold based summit glaciers through direct access to basal ice: A case study constraining the maximum age of Chli Titlis glacier, Switzerland, The Cryosphere Discuss., 2017, 1–15, https://doi.org/10.5194/tc-2017-171, 2017.

Bueler, E. and van Pelt, W.: Mass-conserving subglacial hydrology in the Parallel Ice Sheet Model version 0.6, Geosci. Model Dev., 8,
30 1613–1635, https://doi.org/10.5194/gmd-8-1613-2015, 2015.

Bueler, E., Lingle, C. S., and Brown, J.: Fast computation of a viscoelastic deformable Earth model for ice-sheet simulations, Ann. Glaciol., 46, 97–105, https://doi.org/10.3189/172756407782871567, 2007.

Buoncristiani, J.-F. and Campy, M.: Quaternary Glaciations in the French Alps and Jura, in: Ehlers et al. (2011), pp. 117–126, https://doi.org/10.1016/b978-0-444-53447-7.00010-6, 2011.

35 Calov, R. and Greve, R.: A semi-analytical solution for the positive degree-day model with stochastic temperature variations, J. Glaciol., 51, 173–175, https://doi.org/10.3189/172756505781829601, 2005.

Castiglioni, B.: L'Italia nell'età quaternaria. Carta delle Alpi nel Glaciale, 1940.

Chamberlin, T. C.: Glacial phenomena of North America, in: The great ice age, edited by Geikie, J., pp. 724–775, Stanford, London, 3 edn., 1894.

Charpentier, J. d.: Essai sur les glaciers et sur le terrain erratique du bassin du Rhône, Ducloux, Lausanne, https://doi.org/10.3931/e-rara-8464, 1841.

5   Cohen, D., Gillet-Chaulet, F., Haeberli, W., Machguth, H., and Fischer, U. H.: Numerical reconstructions of the flow and basal conditions of the Rhine glacier, European Central Alps, at the Last Glacial Maximum, The Cryosphere Discuss., 2017, 1–42, https://doi.org/10.5194/tc-2017-204, 2017.

Cossart, E., Fort, M., Bourlès, D., Braucher, R., Perrier, R., and Siame, L.: Deglaciation pattern during the Lateglacial/Holocene transition in the southern French Alps. Chronological data and geographical reconstruction from the Clarée Valley (upper Durance catchment, 10   southeastern France), Palaeogeogr., Palaeoclimatol., Palaeoecol., 315-316, 109–123, https://doi.org/10.1016/j.palaeo.2011.11.017, 2012.

Coutterand, S.: Etude géomorphologique des flux glaciaires dans les Alpes nord-occidentales au Pléistocène récent : du maximum de la dernière glaciation aux premières étapes de la déglaciation, Ph.D. thesis, Université de Savoie, 2010.

Cuffey, K. M. and Paterson, W. S. B.: The physics of glaciers, Elsevier, Amsterdam, 2010.

Dahl-Jensen, D., Johnsen, S. J., Hammer, C. U., Clausen, H. B., and Jouzel, J.: Past Accumulation rates derived from observed annual layers 15   in the GRIP ice core from Summit, Central Greenland, in: Ice in the Climate System, edited by Peltier, W., vol. I12 of *NATO ASI Series*, pp. 517–532, https://doi.org/10.1007/978-3-642-85016-5_29, 1993.

Dansgaard, W., Johnsen, S. J., Clausen, H. B., Dahl-Jensen, D., Gundestrup, N. S., Hammer, C. U., Hvidberg, C. S., Steffensen, J. P., Sveinbjörnsdottir, A. E., Jouzel, J., and Bond, G.: Evidence for general instability of past climate from a 250-kyr ice-core record, Nature, 364, 218–220, https://doi.org/10.1038/364218a0, data archived at the World Data Center for Paleoclimatology, Boulder, Colorado, USA., 20   1993.

de Saussure, H.-B.: Voyages dans les Alpes, précédés d'un essai sur l'histoire naturelle des environs de Genève, vol. 1, Fauche-Borel, Neuchâtel, 1779.

Dee, D. P., Uppala, S. M., Simmons, A. J., Berrisford, P., Poli, P., Kobayashi, S., Andrae, U., Balmaseda, M. A., Balsamo, G., Bauer, P., Bechtold, P., Beljaars, A. C. M., van de Berg, L., Bidlot, J., Bormann, N., Delsol, C., Dragani, R., Fuentes, M., Geer, A. J., Haimberger, L., 25   Healy, S. B., Hersbach, H., Hólm, E. V., Isaksen, L., Kållberg, P., Köhler, M., Matricardi, M., McNally, A. P., Monge-Sanz, B. M., Morcrette, J.-J., Park, B.-K., Peubey, C., de Rosnay, P., Tavolato, C., Thépaut, J.-N., and Vitart, F.: The ERA-Interim reanalysis: configuration and performance of the data assimilation system, Q. J. Roy. Meteor. Soc., 137, 553–597, https://doi.org/10.1002/qj.828, 2011.

Ehlers, J., Gibbard, P. L., and Hughes, P. D., eds.: vol. 15 of *Dev. Quaternary Sci.*, Elsevier, Amsterdam, 2011.

Emiliani, C.: Pleistocene Temperatures, J. Geol., 63, 538–578, https://doi.org/10.1086/626295, 1955.

30   Fabel, D., Ballantyne, C. K., and Xu, S.: Trimlines, blockfields, mountain-top erratics and the vertical dimensions of the last British–Irish Ice Sheet in NW Scotland, qsr, 55, 91–102, https://doi.org/10.1016/j.quascirev.2012.09.002, 2012.

Federici, P. R., Ribolini, A., and Spagnolo, M.: Glacial history of the Maritime Alps from the Last Glacial Maximum to the Little Ice Age, Geol. Soc. Spec. Publ., 433, 137–159, https://doi.org/10.1144/SP433.9, 2017.

Florineth, D.: Surface geometry of the Last Glacial Maximum (LGM) in the Southeastern Swiss Alps (Graubünden) and its paleoclimato-35   logical significance, Eiszeitalter und Gegenwart, 48, https://doi.org/10.3285/eg.48.1.03, 1998.

Florineth, D. and Schlüchter, C.: Reconstructing the Last Glacial Maximum (LGM) ice surface geometry and flowlines in the Central Swiss Alps, Eclogae geol. Helv, 91, 391–407, 1998.

Forbes, J. D.: Illustrations of the Viscous Theory of Glacier Motion. Part III, Philos. T. R. Soc., 136, 177–210, https://doi.org/10.1098/rstl.1846.0015, 1846.

Glen, J.: Experiments on the deformation of ice, J. Glaciol., 2, 111–114, 1952.

Golledge, N. R., Mackintosh, A. N., Anderson, B. M., Buckley, K. M., Doughty, A. M., Barrell, D. J., Denton, G. H., Vandergoes, M. J., Andersen, B. G., and Schaefer, J. M.: Last Glacial Maximum climate in New Zealand inferred from a modelled Southern Alps icefield, Quaternary Res., 46, 30–45, https://doi.org/10.1016/j.quascirev.2012.05.004, 2012.

Goutorbe, B., Poort, J., Lucazeau, F., and Raillard, S.: Global heat flow trends resolved from multiple geological and geophysical proxies, Geophys. J. Int., 187, 1405–1419, https://doi.org/10.1111/j.1365-246x.2011.05228.x, 2011.

Greve, R.: A continuum-mechanical formulation for shallow polythermal ice sheets, Philos. T. R. Soc. A, 355, 921–974, https://doi.org/10.1098/rsta.1997.0050, 1997.

Haeberli, W. and Schlüchter, C.: Geological evidence to constrain modelling of the Late Pleistocene Rhonegletscher (Switzerland), in: The physical basis of ice sheet modelling (Proceedings of the Vancouver Symposium), vol. 170 of *IAHS Publ.*, pp. 333–346, 1987.

Haldimann, P., Graf, H., and Jost, J.: Geological map Bülach (LK 1071), Bundesamt für Landestopografie swisstopo, 2017.

Hantke, R.: Eiszeitalter : Kalt-/Warmzeit-Zyklen und Eistransport im alpinen und voralpinen Raum, Ott, Bern, 2011.

Hays, J. D., Imbrie, J., and Shackleton, N. J.: Variations in the Earth's Orbit: Pacemaker of the Ice Ages, Sience, 194, 1121–1132, https://doi.org/10.1126/science.194.4270.1121, 1976.

Heyman, B. M., Heyman, J., Fickert, T., and Harbor, J. M.: Paleo-climate of the central European uplands during the last glacial maximum based on glacier mass-balance modeling, Quaternary Res., 79, 49–54, https://doi.org/10.1016/j.yqres.2012.09.005, 2013.

Heyman, J., Stroeven, A. P., Harbor, J. M., and Caffee, M. W.: Too young or too old: Evaluating cosmogenic exposure dating based on an analysis of compiled boulder exposure ages, Earth Planet. Sc. Lett., 302, 71–80, https://doi.org/10.1016/j.epsl.2010.11.040, 2011.

Hijmans, R. J., Cameron, S. E., Parra, J. L., Jones, P. G., and Jarvis, A.: Very high resolution interpolated climate surfaces for global land areas, Int. J. Climatol., 25, 1965–1978, https://doi.org/10.1002/joc.1276, 2005.

Hock, R.: Temperature index melt modelling in mountain areas, J. Hydrol., 282, 104–115, https://doi.org/10.1016/S0022-1694(03)00257-9, 2003.

Husen, D. v. and Reitner, J. M.: An Outline of the Quaternary Stratigraphy of Austria, E&G – Quat. Sci. J., 60, 366–387, https://doi.org/10.23689/fidgeo-1764, 2011.

Huss, M. and Farinotti, D.: Distributed ice thickness and volume of all glaciers around the globe, J. Geophys. Res. Earth Surf., 117, F04 010, https://doi.org/10.1029/2012JF002523, 2012.

Huybrechts, P.: Report of the third EISMINT workshop on model intercomparison, Tech. rep., Grindelwald, Switzerland, 1998.

Huybrechts, P.: Sea-level changes at the LGM from ice-dynamic reconstructions of the Greenland and Antarctic ice sheets during the glacial cycles, Quaternary Sci. Rev., 21, 203–231, https://doi.org/10.1016/s0277-3791(01)00082-8, 2002.

Ivy-Ochs, S.: Glacier variations in the European Alps at the end of the last glaciation, Cuadernos de Investigación Geográfica, 41, 295, https://doi.org/10.18172/cig.2750, 2015.

Ivy-Ochs, S., Kerschner, H., Reuther, A., Preusser, F., Heine, K., Maisch, M., Kubik, P. W., and Schlüchter, C.: Chronology of the last glacial cycle in the European Alps, J. Quaternary Sci., 23, 559–573, https://doi.org/10.1002/jqs.1202, 2008.

Ivy-Ochs, S., Kerschner, H., Maisch, M., Christl, M., Kubik, P. W., and Schlüchter, C.: Latest Pleistocene and Holocene glacier variations in the European Alps, Quaternary Sci. Rev., 28, 2137–2149, https://doi.org/10.1016/j.quascirev.2009.03.009, 2009.

Jäckli, H.: Die Vergletscherung der Schweiz im Würm maximum, Eclogae geol. Helv, 55, 1962.

Jarvis, A., Reuter, H., Nelson, A., and Guevara, E.: Hole-filled SRTM for the globe Version 4, available from the CGIAR-CSI SRTM 90m Database, http://srtm.csi.cgiar.org, 2008.

Johnsen, S. J., Dahl-Jensen, D., Dansgaard, W., and Gundestrup, N.: Greenland palaeotemperatures derived from GRIP bore hole temperature and ice core isotope profiles, Tellus B, 47, 624–629, https://doi.org/10.1034/j.1600-0889.47.issue5.9.x, 1995.

5   Jouvet, G., Seguinot, J., Ivy-Ochs, S., and Funk, M.: Modelling the diversion of erratic boulders by the Valais Glacier during the last glacial maximum, J. Glaciol., 63, 487–498, https://doi.org/10.1017/jog.2017.7, 2017.

Jouzel, J., Masson-Delmotte, V., Cattani, O., Dreyfus, G., Falourd, S., Hoffmann, G., Minster, B., Nouet, J., Barnola, J. M., Chappellaz, J., Fischer, H., Gallet, J. C., Johnsen, S., Leuenberger, M., Loulergue, L., Luethi, D., Oerter, H., Parrenin, F., Raisbeck, G., Raynaud, D., Schilt, A., Schwander, J., Selmo, E., Souchez, R., Spahni, R., Stauffer, B., Steffensen, J. P., Stenni, B., Stocker, T. F., Tison, J. L.,
10   Werner, M., and Wolff, E. W.: Orbital and Millennial Antarctic Climate Variability over the Past 800,000 Years, Sience, 317, 793–796, https://doi.org/10.1126/science.1141038, data archived at the World Data Center for Paleoclimatology, Boulder, Colorado, USA., 2007.

Keller, O. and Krayss, E.: Mittel- und spätpleistozäne Stratigraphie und Morphogenese in Schlüsselregionen der Nordschweiz, E&G – Quat. Sci. J., 59, https://doi.org/10.23689/fidgeo-1026, 2010.

Kelly, M. A., Buoncristiani, J.-F., and Schlüchter, C.: A reconstruction of the last glacial maximum (LGM) ice surface geometry in the
15   western Swiss Alps and contiguous Alpine regions in Italy and France, Eclogae geol. Helv, pp. 57–75, 2004.

Kleman, J.: Preservation of landforms under ice sheets and ice caps, Geomorphology, 9, 19–32, https://doi.org/10.1016/0169-555x(94)90028-0, 1994.

Kleman, J. and Borgström, I.: Glacial land forms indicative of a partly frozen bed, J. Glaciol., 40, 255–264, https://doi.org/10.1017/S0022143000007346, 1994.

20   Kleman, J., Hättestrand, C., Stroeven, A. P., Jansson, K. N., De Angelis, H., and Borgström, I.: Reconstruction of Palaeo-Ice Sheets – Inversion of their Glacial Geomorphological Record, in: Glacier Science and Environmental Change, edited by Knight, P. G., pp. 192–198, Blackwell, Malden, MA, https://doi.org/10.1002/9780470750636.ch38, 2006.

Kleman, J., Jansson, K., De Angelis, H., Stroeven, A., Hättestrand, C., Alm, G., and Glasser, N.: North American ice sheet build-up during the last glacial cycle, 115–21 kyr, Quaternary Sci. Rev., 29, 2036–2051, https://doi.org/10.1016/j.quascirev.2010.04.021, 2010.

25   Lingle, C. S. and Clark, J. A.: A numerical model of interactions between a marine ice sheet and the solid Earth: application to a West Antarctic ice stream, J. Geophys. Res., 90, 1100–1114, https://doi.org/10.1029/JC090iC01p01100, 1985.

Link, A. and Preusser, F.: Hinweise auf eine Vergletscherung des Kemptener Beckens während des Mittelwürms, Eiszeitalter und Gegenwart, 55, 65–88, https://doi.org/10.3285/eg.55.1, 2006.

Lisiecki, L. E. and Raymo, M. E.: A Pliocene-Pleistocene stack of 57 globally distributed benthic δ^{18}O records, Paleoceanography, 20,
30   PA1003, https://doi.org/10.1029/2004pa001071, 2005.

Lliboutry, L. A. and Duval, P.: Various isotropic and anisotropic ices found in glaciers and polar ice caps and their corresponding rheologies, Ann. Geophys., 3, 207–224, 1985.

Ludwig, P., Schaffernicht, E. J., Shao, Y., and Pinto, J. G.: Regional atmospheric circulation over Europe during the Last Glacial Maximum and its links to precipitation, J. Geophys. Res. Atmos., 121, 2130–2145, https://doi.org/10.1002/2015jd024444, 2016.

35   Luetscher, M., Boch, R., Sodemann, H., Spötl, C., Cheng, H., Edwards, R. L., Frisia, S., Hof, F., and Müller, W.: North Atlantic storm track changes during the Last Glacial Maximum recorded by Alpine speleothems, Nature Communications, 6, 6344, https://doi.org/10.1038/ncomms7344, 2015.

Lüthi, M., Funk, M., Iken, A., Gogineni, S., and Truffer, M.: Mechanisms of fast flow in Jakobshavns Isbræ, Greenland; Part III: measurements of ice deformation, temperature and cross-borehole conductivity in boreholes to the bedrock, J. Glaciol., 48, 369–385, https://doi.org/10.3189/172756502781831322, 2002.

Martrat, B., Grimalt, J. O., Shackleton, N. J., de Abreu, L., Hutterli, M. A., and Stocker, T. F.: Four climate cycles of recurring deep and
5   surface water destabilizations on the Iberian margin, Sience, 317, 502–507, https://doi.org/10.1126/science.1139994, 2007.

Mesinger, F., DiMego, G., Kalnay, E., Mitchell, K., Shafran, P. C., Ebisuzaki, W., Jović, D., Woollen, J., Rogers, E., Berbery, E. H., Ek, M. B., Fan, Y., Grumbine, R., Higgins, W., Li, H., Lin, Y., Manikin, G., Parrish, D., and Shi, W.: North American regional reanalysis, B. Am. Meteorol. Soc., 87, 343–360, https://doi.org/10.1175/BAMS-87-3-343, 2006.

Mey, J., Scherler, D., Wickert, A. D., Egholm, D. L., Tesauro, M., Schildgen, T. F., and Strecker, M. R.: Glacial isostatic uplift of the European
10   Alps, Nature Communications, 7, 13 382, https://doi.org/10.1038/ncomms13382, 2016.

Monegato, G., Ravazzi, C., Donegana, M., Pini, R., Calderoni, G., and Wick, L.: Evidence of a two-fold glacial advance during the last glacial maximum in the Tagliamento end moraine system (eastern Alps), Quaternary Res., 68, 284–302, https://doi.org/10.1016/j.yqres.2007.07.002, 2007.

Monegato, G., Scardia, G., Hajdas, I., Rizzini, F., and Piccin, A.: The Alpine LGM in the boreal ice-sheets game, Sci. Rep., 7, 2078,
15   https://doi.org/10.1038/s41598-017-02148-7, 2017.

Nye, J. F.: The Flow Law of Ice from Measurements in Glacier Tunnels, Laboratory Experiments and the Jungfraufirn Borehole Experiment, Proc. R. Soc. London, Ser. A, 219, 477–489, 1953.

Onde, H.: La Maurienne et la Tarentaise ; étude de Géographie physique, Ph.D. thesis, Université de Grenoble, 1938.

Paterson, W. S. B. and Budd, W. F.: Flow parameters for ice sheet modeling, Cold Reg. Sci. Technol., 6, 175–177, 1982.

20 Patterson, T. and Kelso, N. V.: Natural Earth. Free vector and raster map data, http://naturalearthdata.com, 2017.

Penck, A. and Brückner, E.: Die alpen im Eiszeitalter, Tauchnitz, Leipzig, 1909.

Preusser, F.: Towards a chronology of the Late Pleistocene in the northern Alpine Foreland, Boreas, 33, 195–210, https://doi.org/10.1111/j.1502-3885.2004.tb01141.x, 2004.

Preusser, F. and Schlüchter, C.: Dates from an important early Late Pleistocene ice advance in the Aare valley, Switzerland, Eclogae geol.
25   Helv, 97, 245–253, https://doi.org/10.1007/s00015-004-1119-4, 2004.

Preusser, F., Geyh, M. A., and Schlüchter, C.: Timing of Late Pleistocene climate change in lowland Switzerland, Quaternary Sci. Rev., 22, 1435 – 1445, https://doi.org/10.1016/S0277-3791(03)00127-6, 2003.

Preusser, F., Blei, A., Graf, H. R., and Schlüchter, C.: Luminescence dating of Würmian (Weichselian) proglacial sediments from Switzerland: methodological aspects and stratigraphical conclusions, Boreas, 36, 130–142, https://doi.org/10.1111/j.1502-3885.2007.tb01187.x, 2007.

30 Preusser, F., Graf, H. R., Keller, O., Krayss, E., and Schlüchter, C.: Quaternary glaciation history of northern Switzerland, Quaternary Sci. J., 60, 282–305, https://doi.org/10.3285/eg.60.2-3.06, 2011.

Schlüchter, C.: A non-classical summary of the Quaternary stratigraphy in the northern alpine foreland of Switzerland, Bull. Soc. neuchâteloise géogr., 32, 143–157, 1988.

Schlüchter, C.: Fazies und Chronologie des letzteiszeitlichen Eisaufbaues im Alpenvorland der Schweiz. In Klimageschichtliche Probleme
35   der letzten 130000 Jahre, in: Klimageschichtliche Probleme der letzten 130 000 Jahre, edited by Frenzel, B., pp. 401–407, G. Fischer Verlag, Stuttgart, 1991.

Seguinot, J.: Spatial and seasonal effects of temperature variability in a positive degree-day glacier surface mass-balance model, J. Glaciol., 59, 1202–1204, https://doi.org/10.3189/2013JoG13J081, 2013.

Seguinot, J.: Numerical modelling of the Cordilleran ice sheet, Ph.D. thesis, Stockholm University, http://urn.kb.se/resolve?urn=urn:nbn:se:
    su:diva-106815, 2014.

Seguinot, J., Khroulev, C., Rogozhina, I., Stroeven, A. P., and Zhang, Q.: The effect of climate forcing on numerical simulations of the
    Cordilleran ice sheet at the Last Glacial Maximum, The Cryosphere, 8, 1087–1103, https://doi.org/10.5194/tc-8-1087-2014, 2014.

5 Seguinot, J., Rogozhina, I., Stroeven, A. P., Margold, M., and Kleman, J.: Numerical simulations of the Cordilleran ice sheet through the last
    glacial cycle, The Cryosphere, 10, 639–664, https://doi.org/10.5194/tc-10-639-2016, 2016.

Shackleton, N. J. and Opdyke, N. D.: Oxygen isotope and palaeomagnetic stratigraphy of Equatorial Pacific core V28-238: Oxygen isotope
    temperatures and ice volumes on a 10^5 year and 10^6 year scale, Quaternary Res., 3, 39–55, https://doi.org/10.1016/0033-5894(73)90052-5,
    1973.

10 Spötl, C. and Mangini, A.: Stalagmite from the Austrian Alps reveals Dansgaard–Oeschger events during isotope stage 3:: Implications for
    the absolute chronology of Greenland ice cores, Earth Planet. Sc. Lett., 203, 507–518, https://doi.org/10.1016/S0012-821X(02)00837-3,
    2002.

Strandberg, G., Brandefelt, J., Kjellstrom, E., and Smith, B.: High-resolution regional simulation of last glacial maximum climate in Europe,
    Tellus A, 63, 107–125, https://doi.org/10.1111/j.1600-0870.2010.00485.x, 2011.

15 Stroeven, A. P., Fabel, D., Hättestrand, C., and Harbor, J.: A relict landscape in the centre of Fennoscandian glaciation: cosmogenic radionu-
    clide evidence of tors preserved through multiple glacial cycles, geom, 44, 145–154, https://doi.org/10.1016/S0169-555X(01)00150-7,
    2002.

Suter, S., Laternser, M., Haeberli, W., Frauenfelder, R., and Hoelzle, M.: Cold firn and ice of high-altitude glaciers in the Alps: measurements
    and distribution modelling, J. Glaciol., 47, 85–96, https://doi.org/10.3189/172756501781832566, 2001.

20 the PISM authors: PISM, a Parallel Ice Sheet Model, http://www.pism-docs.org, 2017.

Tulaczyk, S., Kamb, W. B., and Engelhardt, H. F.: Basal mechanics of Ice Stream B, west Antarctica: 1. Till mechanics, J. Geophys. Res.,
    105, 463, https://doi.org/10.1029/1999jb900329, 2000.

van Husen, D.: Zur quartären Entwicklung im Gailtal, in: Arbeitstagung der Geologischen Bundesanstalt, pp. 10–15, Geologische Bunde-
    sanstalt, Wien, http://www.geologie.ac.at/de/GEOMARKT/arbeitstagungen.html, 1985.

25 van Husen, D.: Die Ostalpen in den Eiszeiten, Geologische Bundesanstalt, Wien, 1987.

van Husen, D.: Quaternary Glaciations in Austria, in: Ehlers et al. (2011), pp. 15–28, https://doi.org/10.1016/b978-0-444-53447-7.00002-7,
    2011.

Venetz, I.: Mémoire sur les variations de la température dans les Alpes de la Suisse, 1821.

Windham, W. and Martel, P.: An account of the glacières or ice alps in Savoy, in two letters, one from an English gentleman to his friend at
30   Geneva; the other from Peter Martel, engineer, to the said English gentleman, as laid before the Royal Society, London, printed for Peter
    Martel, 1744.

Winkelmann, R., Martin, M. A., Haseloff, M., Albrecht, T., Bueler, E., Khroulev, C., and Levermann, A.: The Potsdam Parallel Ice Sheet
    Model (PISM-PIK) – Part 1: model description, The Cryosphere, 5, 715–726, https://doi.org/10.5194/tc-5-715-2011, 2011.

Wirsig, C., Zasadni, J., Christl, M., Akçar, N., and Ivy-Ochs, S.: Dating the onset of LGM ice surface lowering in the High Alps, Quaternary
35   Sci. Rev., 143, 37–50, https://doi.org/10.1016/j.quascirev.2016.05.001, https://doi.org/10.1016/j.quascirev.2016.05.001, 2016.

Wohlfarth, B., Veres, D., Ampel, L., Lacourse, T., Blaauw, M., Preusser, F., Andrieu-Ponel, V., Kéravis, D., Lallier-Vergès, E., Björck,
    S., Davies, S. M., de Beaulieu, J.-L., Risberg, J., Hormes, A., Kasper, H. U., Possnert, G., Reille, M., Thouveny, N., and Zander, A.:

Rapid ecosystem response to abrupt climate changes during the last glacial period in western Europe, 40–16 ka, Geology, 36, 407, https://doi.org/10.1130/G24600A.1, 2008.

Wu, H. B., Guiot, J. L., Brewer, S., and Guo, Z. T.: Climatic changes in Eurasia and Africa at the last glacial maximum and mid-Holocene: reconstruction from pollen data using inverse vegetation modelling, Clim. Dynam., 29, 211–229, 2007.

5 Ziemen, F. A., Hock, R., Aschwanden, A., Khroulev, C., Kienholz, C., Melkonian, A., and Zhang, J.: Modeling the evolution of the Juneau Icefield between 1971 and 2100 using the Parallel Ice Sheet Model (PISM), J. Glaciol., 62, 199–214, https://doi.org/10.1017/jog.2016.13, 2016.